LUND UNIVERSITY

A numerical study of mixing phenomena and reaction front propagation in partially premixed combustion engines

Ibron, Christian

2019

Document Version:
Publisher's PDF, also known as Version of record

Link to publication

Citation for published version (APA):
Ibron, C. (2019). *A numerical study of mixing phenomena and reaction front propagation in partially premixed combustion engines.* [Doctoral Thesis (compilation), Department of Energy Sciences]. Department of Energy Sciences, Lund University.

Total number of authors:
1

Creative Commons License:
Unspecified

General rights
Unless other specific re-use rights are stated the following general rights apply:
Copyright and moral rights for the publications made accessible in the public portal are retained by the authors and/or other copyright owners and it is a condition of accessing publications that users recognise and abide by the legal requirements associated with these rights.
• Users may download and print one copy of any publication from the public portal for the purpose of private study or research.
• You may not further distribute the material or use it for any profit-making activity or commercial gain
• You may freely distribute the URL identifying the publication in the public portal

Read more about Creative commons licenses: https://creativecommons.org/licenses/

Take down policy
If you believe that this document breaches copyright please contact us providing details, and we will remove access to the work immediately and investigate your claim.

LUND UNIVERSITY

PO Box 117
221 00 Lund
+46 46-222 00 00

A numerical study of mixing phenomena and reaction front propagation in partially premixed combustion engines

CHRISTIAN IBRON
FACULTY OF ENGINEERING | LUND UNIVERSITY

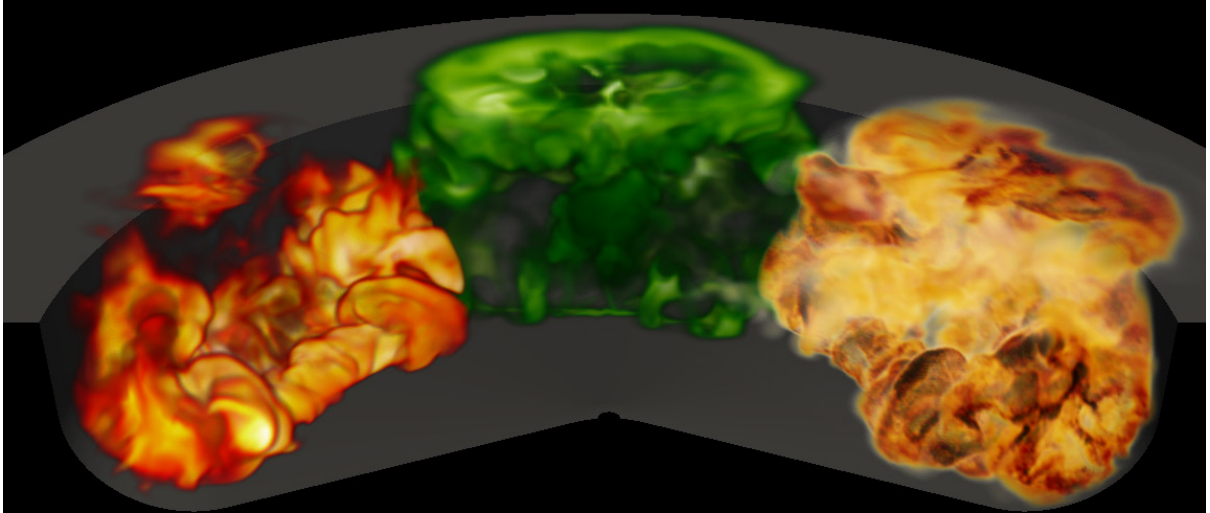

A numerical study of mixing phenomena and reaction front propagation in partially premixed combustion engines

A numerical study of mixing phenomena and reaction front propagation in partially premixed combustion engines

by Christian Ibron

LUND
UNIVERSITY

Thesis for the degree of Doctor of Philosophy
Thesis advisors: Prof. Xue-Song Bai, Dr. Hessamedin Fatehi, Dr. Mehdi Jangi
Faculty opponent: Dr. Arnaud Mura

To be presented, with the permission of the Faculty of Engineering of Lund University, for public criticism in the lecture hall M:B, M-building, at the Department of Energy Sciences on the 13th of December 2019 at 10:00.

Organization	Document name
LUND UNIVERSITY Department of Energy Sciences Box 118 SE–221 00 LUND Sweden	DOCTORAL DISSERTATION
	Date of disputation 2019-12-13
	Sponsoring organization
Author(s) Christian Ibron	

Title and subtitle

A numerical study of mixing phenomena and reaction front propagation in partially premixed combustion engines

Abstract

This work treats the modelling of PPC engine combustion through 3D computational fluid dynamics. In order to develop a cost-effective CFD model for the design and performance analysis of PPC engines it is important to first understand the multiple modes of combustion in PPC engines, e.g., the onset of the first ignition kernels, the propagation of the ignition/flame fronts, and the effect of charge stratification on the combustion process. To this end the mixing process and incylinder turbulent flow are studied in the first part of the thesis. The results of the study, which are covered in papers I and III, show that the swirling flow structure generated in the intake stroke loses non-axial components in later stages, which supports the use of sector mesh in the combustion stroke CFD simulations. The sector simulations show similar behaviour in terms of spray induced momentum and fuel distribution compared to a full cylinder simulation as long as the mixing occurs far from the cylinder center. In the second part of the thesis, CFD simulations of the combustion process are performed, based on a direct coupling of the finite rate chemistry with the flow transport. Different models for turbulence/chemistry interaction are considered; the model based on well-stirred reactors and partially stirred reactors, and the model based on transported probability density function within the Eulerian Stochastic Fields (PDF-ESF). These models are used to analyse the mixed mode combustion process in an experimental PPC engine. The LES models are shown to be able to resolve sufficient scalar stratification to properly represent the combustion phasing of the ignition front combustion mode. While the LES-ESF shows better predictions of the required inlet temperatures, the model is computational more demanding than the well-stirred/partially stirred reactor models – the computational time increases with the number of stochastic fields.

Key words

CFD,PPC,Ignition front,ICE

Classification system and/or index terms (if any)

Supplementary bibliographical information	Language English
ISSN and key title 0282-1990	ISBN 978-91-7895-322-6 (print) 978-91-7895-323-3 (pdf)
Recipient's notes	Number of pages 98 / Price
	Security classification

I, the undersigned, being the copyright owner of the abstract of the above-mentioned dissertation, hereby grant to all reference sources the permission to publish and disseminate the abstract of the above-mentioned dissertation.

Signature 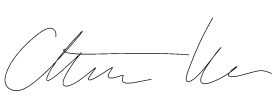 Date 2019-11-19

DOKUMENTDATABLAD enl SIS 61 41 21

A numerical study of mixing phenomena and reaction front propagation in partially premixed combustion engines

by Christian Ibron

LUND
UNIVERSITY

Funding information: The thesis work was financially supported by the members of the Competence Center for Combustion Processes (KCFP) at Lund university and the Swedish Energy Agency (Energimyndigheten).

Cover illustration: Ignition front propagation in a PPC engine. Temperature on the left, formaldehyde in the middle and heat release rate on the right.

© Christian Ibron 2019

Department of Energy Sciences
Faculty of Engineering
Lund University
Box 118
SE–221 00 LUND
Sweden

ISBN: 978-91-7895-322-6 (print)
ISBN: 978-91-7895-323-3 (pdf)
ISSN: 0282-1990
ISRN: LUTMDN/TMHP-19/1155-SE

Printed in Sweden by Media-Tryck, Lund University, Lund 2019

Tillägnas min familj
Linda – William – Leonie – Alice

Contents

List of publications

This thesis is based on the following publications, referred to by their Roman numerals:

I **Numerical estimation of asymmetry of in-cylinder flow in a light duty direct injection engine with re-entrant piston bowl**

C. Ibron, M. Jangi, T. Lucchini, XS. Bai
SAE Technical Paper, 2017-01-2209

II **Effect of injection timing on the ignition and mode of combustion in a HD PPC engine running low load**

C. Ibron, M. Jangi, XS. Bai
SAE Technical Paper, 2019-01-0211

III **Effects of in-cylinder flow simplifications on turbulent mixing at varying injection timings in a piston bowl PPC engine**

C. Ibron, M. Jangi, XS. Bai
SAE Technical Paper, 2019-01-0220

IV **Large eddy simulation of an ignition front in a heavy duty partially premixed combustion engine**

C. Ibron, H. Fatehi, M. Jangi, XS. Bai
SAE Technical Paper, 2019-01-0211

V **Numerical simulation of a mixed-mode reaction front in a PPC engine**

C. Ibron, H. Fatehi, Z. Wang, P. Stamatoglou, M. Lundgren, M. Aldén, M. Richter, Ö. Andersson, XS. Bai
Manuscript submitted to the 38th International Symposium on Combustion

Acknowledgements

This work was carried out at the Department of Energy Sciences, Lund University, Sweden. The thesis work was financially supported by the members of the competence center for combustion processes (KCFP) at Lund university and the Swedish energy agency (Energimyndigheten). Computational resources were provided by Swedish National Infrastructure for Computing (SNIC) at PDC and HPC2N.

The first big thanks goes to my main supervisor, Prof. Xue-Song Bai, who, with divine patience, has mentored me and helped me to obtain the necessary knowledge to finish my work. Thank you for giving me this opportunity and for all the kindness, support and time you spent on my account. A great thanks goes to my co-supervisors Dr. Mehdi Jangi and Dr. Hesameddin Fatehi. You've helped me with understanding, coding, formulations, as well as the constructive criticism which greatly improved my work. I would like give my colleagues Dr. Thommie Nilsson, Mateusz, Hamed and Dr. Ali al-Sam a very special thanks for all the discussions (silly and otherwise), the encouragement and support. Without you it would have been a lot harder or maybe even impossible. A special thanks goes to my room-mates Senbin and Dr. Cheng Gong who taught me a lot about Chinese culture, turbulent combustion and how to properly take a power-nap. I would also like to thank my other colleagues at the division: Dr. Rixin Yu, Shijie, Leilei, Michael, Morteza, Monika, Francesco, Mark and Shenghui for your support. Thanks to Dr. Daniel Moëll who shared a traumatic week in a 1.5 m^2 dormitory room with Mateusz, me and two other guys. An extra thanks goes to Dr. Robert Szasz and Prof. Johan Revstedt who helped me a lot with understanding the underlying physics and numerics. I would like to thank the previous generation of PhD students for the crash courses in turbulent combustion. I would also like to give my colleagues at the other departments a big thanks for the help and discussions. Particularly Dr. Sara Lönn, Dr. Zhenkan Wang, Dr. Marcus Lundgren and Panagiotta who have provided me with experimental data and good scientific discussions. Dr. Erik Svensson and Dr. Nhut Lam have been a great support for me in my learning process. Extra thanks to Niko, Vikram, Nika, Dr. Kenan Muric and the senior staff at combustion engines; Professors Öivind, Per, Sebastian and Martin. Thanks for your patience and great knowledge. Thank you professors Magnus Genrup, Marcus Thern and Jens Klingmann for the jokes and discussions, and thank you Catarina for all the patience. I would also like to thank Prof. Tommaso Lucchini at Politechnico di Milano for his help with OpenFOAM and LibICE.

Most of all I would like to thank my family. First I thank my wife Linda to whom I owe my happiness. Then my children William, Leonie and Alice. I'm sorry I had to work so much. Finally I thank my sister and my parents, Natalie, Grażyna and Waldemar, for their support when things are tough.

Nomenclature

PPC	partially premixed combustion
HCCI	homogeneous charge compression ignition
LTC	low temperature combustion
TDC	top dead center
aTDC	after top dead center
CFD	computational fluid dynamics
LES	large eddy simulation
RAS	Reynolds average simulation
PaSR	partially stirred reactor
WSR	well stirred reactor
ICE	internal combustion engine
CDC	conventional Diesel combustion
NO_x	nitrogen oxides
PIV	particle image velocimetry
SOI	start of injection
SOC	start of combustion
UHC	unburned hydrocarbon
PRF	primary reference fuel
PRF87	PRF with 87% iso-octane by volume
SI	spark ignition
CI	compression ignition
ESF	Eulerian stochastic fields
τ_i	ignition delay time
CA	crank angle
CA50	crank angle at which 50% of the heat is released

Populärvetenskaplig sammanfattning

Trots hotet om global uppvärmning och giftiga utsläpp fortsätter världsekonomin att drivas av förbränningsmotorer - en majoritet av alla självgående transportmedel har en förbränningsmotor i sig. Det kommer sannolikt att förbli så ett bra tag eftersom klimatvänligare alternativ bara finns tillgängliga i ett fåtal länder där tillverkningen av elektrisk energi inte sker genom förbränning av kolväten. Sett ur ett globalt perspektiv tillverkas mer än 80 % av vår energi genom att bränna kolväten av något slag. Detta gör att i de flesta länder har elektrifierade fordon koldioxidutsläppsvärden som ligger i samma stroleksordning som de från fordon drivna av förbränningsmotorer. Även om västvärlden försöker ställa om till en mer klimatvänlig elmix så ökar konsumtionen av kolväten i utvecklingsländerna. I slutändan innebär detta att utvecklingen av förbränningsmotorer är avgörande för att minska transportsektorns klimat- och miljö-påverkan.

De senaste decennierna har ett antal nya förbränningsmotorkoncept introducerats som alternativ till de vanligt förekommande Diesel- och bensin-motorerna. Dessa koncept har som gemensam nämnare att de försöker bränna bränslet vid lägre temperaturer än traditionella förbränningsmotorer. Detta har i sin tur ett antal positiva följder som lägre värmeförluster, lägre utsläpp av giftiga kväveoxider (NO_x), lägre utsläpp av sot och minskad bränsleförbrukning. Tyvärr har de nya motorkoncepten även vissa nackdelar som exempelvis instabilt beteende vid hög belastning eller ofullständig förbränning vid alltför låg belastning. För att vidareutveckla koncepten och undvika nämnda problem behövs mer kunskap.

Arbetet som beskrivs i denna avhandling är ämnat att förbättra förmågan att med hjälp av datorer och matematik kunna återskapa en digital version av den process som sker när bränsle brinner i en förbränningsmotor, en så kallad tredimensionell CFD-simulering (Computational Fluid Dynamics) av förbränningsprocessen. Så länge simuleringen är tillräckligt noggrann kan man därefter mäta och studera hur förbränningsprocessen fungerar i detalj. För att kunna uppnå tillräcklig noggrannhet i simuleringen krävs dock god kunskap om hur en sådan simuleringsmodell ska byggas.

Förbränning i motorer är till mycket hög grad beroende av transport av molekyler och värme i gaser. I en 3D-CFD simulering av en förbränningsmotor studerar man lite förenklat hur rörelser i gasen samverkar med förbränningen, men detta kräver såklart god förståelse för hur gasen rör sig till att börja med. En del av det arbete som presenteras i denna avhandling tittar på hur man väljer att beskriva flödet. I början av en simulering måste man t.ex. gissa sig till hur flödet ser ut och en del av arbetet går ut på att studera effekten av olika sådana gissningar. Likaså studeras vad som händer när man minskar storleken av den simulerade volymen genom att anta symmetriskt beteende i någon riktning. Resultaten från dessa studier visar att förenklade flöden och symmetriska antaganden ibland vara bra, beroende på hur motorn körs.

Inuti förbränningsmotorer rör sig gasen med väldigt höga hastigheter - detta gör att storleken på virvlarna i gasen varierar från samma storleksordning som själva motorcylindern till några miljondelar av en meter. För att fånga effekterna från de minsta virvlarna behövs extremt mycket datorkraft (så kallade direkta numeriska simuleringar eller DNS) vilket man i dagsläget inte har möjlighet att applicera på motorer. Istället introduceras så kallade turbulensmodeller som på olika sätt väljer att bortse från de små virvlarna när gasens rörelser beräknas och istället lägger till effekten från virvlarna i ett separat skede. Detta snabbar upp simuleringarna tillräckligt för att de ska gå att genomföra men innebär att man på ett eller annat sätt måste anta på vilket sätt de små virvlarna påverkat bl.a. förbränningen.

När det handlar om just interaktionen mellan de små virvlarna och förbränningen kallas antagandena för förbränningsmodeller och utgör en väldigt viktig del av hur en motorsimulering är uppbyggd. En majoritet av det arbete som presenteras i denna avhandling studerar hur den typ av förbränningsprocess som uppstår i de nya motorkoncepten ska samverka med de effekterna från de små virvlarna. Avhandlingens resultat visar att när förbränning i de nya motorkoncepten ska simuleras så är det avgörande att man har med information om hur den småskaliga spridningen av viktiga storheter som till exempel temperatur påverkar förbränningen.

Slutligen undersöks hur övergångar mellan olika förbränningsprocesser som uppstår i nya motorkoncept kan hanteras i simuleringar som använder turbulensmodeller. En förslagen metod presenteras och jämförs med experimentiella bilder. Jämförelsen visar att den förslagna metoden lyckas fånga övergångarna i förbränningsprocessen.

Chapter 1

Introduction

This chapter introduces the reader to the subject of the thesis by discussing the role of the reciprocating engine in today's society. The complex and interconnected subjects of CO_2 emissions, the benefits of mechanized transport, alternative drive-lines, and the state of energy generation in the world are described to make the reader understand the research effort.

1.1 Motivation

Mechanised transport is the most fundamental component of a global economy and is a natural part of life in most countries. Thanks to mechanised transport we can take fulfilling jobs that are located more than half a days horse-ride from our home, we can enjoy groceries that are grown at a different latitude than our own and we can cooperate in global industrial and academic endeavours that elevate all of mankind. In other words: modern transport capabilities have made humans happier, more productive, healthier, richer, smarter and most importantly - more pacifistic. The backside to this is the increased usage of energy per capita of a population which enjoys such benefits - a need which continues to grow with the advances of technology. As the global economy equalizes the living standard worldwide the total energy requirement is increasing dramatically [1], which forces us to steadily expand and improve our methods for energy generation.

With the advent of industrialization the energy need and thus emission of carbon has caused atmospheric levels of CO_2 which have not been observed for hundreds of millennia [2]. For this reason, as a direct cause of mankind's improved living standard, the global temperature has increased drastically in what is called the global warming effect. With the advancement of technology alternative methods for power generation have become available including nuclear, sun, wind, hydro and geothermal power - all of which have very low global warming emissions [3]. These methods require considerable investment and re-adaptation of

existing systems to successfully replace the carbon based energy sources, but progress towards climate-friendly energy supply is possible and has become a reality in some countries. While stationary equipment can be connected to an energy grid with small consequences for global warming the transport sector is, for natural reasons, dependent on isolated and mobile energy sources. For the last century this has almost exclusively meant a reciprocating combustion engine fuelled by fossil fuels in land based transport and to a considerable extent in sea based transport as well.

In the last decade climate awareness in the western world has increased to the level that it now is impossible to open a newspaper without encountering it in one way or the other. With the drive to reduce global warming impact from ICEs the manufacturers have focused on maximizing fuel efficiency to reduce CO_2 emissions. Further reduction has been proposed by new fuel types which are not fossil-based and can instead be formed by e.g. atmospheric carbon capture or industrial CO_2 so that no "new" carbon is introduced to the atmosphere [4, 5]. Currently such conversion processes are expensive in terms of energy efficiency but could develop into economically feasible systems for future CO_2-neutral renewable fuels.

In addition to legislative pressure from local governments to reduce CO_2 emissions, engine manufacturers are seeing competition from the electrification of land based vehicles. While the current level of energy storage capacity limits this technology to light duty vehicles or at best short distance, low density consumer goods transports the electrification has shown that there are alternatives to the ICE as the main energy source in the transport sector. The high energy conversion efficiency of electric vehicles beats even the theoretical Carnot efficiency limit of ICEs (at reasonable temperatures) and there are no local emissions from the electric energy conversion.

Despite these benefits vehicle electrification has some notable drawbacks. Firstly the electric energy is only as climate friendly as its method of generation. Since fossil power continues to be the main source of energy throughout the world (cf. figure 1.1) an electrified vehicle has roughly the same energy conversion climate impact as an ICE driven vehicle, if one starts counting from the original state of the energy. Oxidation of hydrocarbon fuel types is responsible for more than 80% [1] of the worlds energy generation and while a small trend in the increased use of renewable sources can be seen in some parts of the world the majority of energy will most likely come from fossil sources in the foreseeable future as well. A second big hindrance for fully electric vehicles is the required production energy for the electric battery. While life cycle analysis research on electric vehicles is limited due to the relative youth of the technology some estimates have shown that only after seven years [6] of driving can the electric vehicle break even with and surpass a new diesel car in CO_2 emissions. This analysis includes estimates of energy costs based on where existing electric batteries are manufactured. Despite these drawbacks there is great potential in vehicle elec-

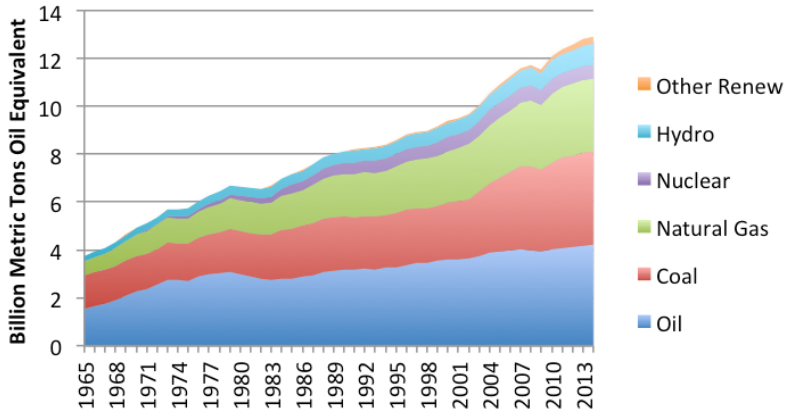

Figure 1.1: The figure depicts the past decades development of primary energy consumption by fuel[1].

trification and hybrid technology allows the best of two worlds, albeit at the cost of two energy sources.

A second promising future mobile energy source is the fuel-cell which utilizes an electrochemical process where fuel (most often hydrogen gas) and oxidizer are combined at low temperatures to generate electricity. No moving parts are needed and the total energy conversion efficiency varies between 40% to 60% [7–10]. As long as reactants are provided to the fuel cell it can continue to operate. The storage of hydrogen is problematic due to the flammability of the gas and its inherent ability to escape confinement. The current generation of fuel-cell vehicles are able to drive distances close to modern diesel cars, but the technology retains a niche market share due to relatively steep price tags. Despite this several production line models have been launched which utilize fuel-cells as an energy source.

With global warming on the one hand and the difficulties of leaving ICEs as an energy source on the other the future of transportation is very hard to predict in the authors opinion. Based on the wide selection of available drive trains in today's vehicle market the vehicle manufacturers surely agree. While the right course is unknown the best thing to do is to prepare for all possible options, and so this thesis has the end goal of further developing the ICE.

Modern ICEs have been continuously developed for more than a hundred years to date, with the spark ignition (SI) engine having been invented by Nicholaus Otto in 1876 and the Diesel engine by Rudolf Diesel in 1892. Both concepts have seen ebbs and flows in popularity but have found their place in the transport sector, with the SI engine dominating the light duty, personal transports, while the diesel engine is more common in heavy duty

systems where the large performance range is sacrificed for fuel efficiency. The SI engine can obtain high speeds which enables it to cover a wide range of operating points and it also emits relatively low levels of local emissions. The Diesel engine at the other hand utilizes compression ignition which enables the usage of high compression ratios. This in turn gives a higher brake efficiency at the cost of local emissions like soot and nitrous oxides (NO_x). The Diesel engine has a slightly slower combustion process and requires bulkier engines which limits how fast the engine can operate.

For the past few decades new engine concepts have been proposed to utilize the best aspects of SI and Diesel engines. Low temperature combustion (LTC) engines are a family of ICE concepts which try to retain the efficiency of high compression ratios while avoiding local emissions like unburned hydrocarbons (UHC), CO, soot and NO_x. While these local emissions can be partially handled by after-treatment systems in existing engine concepts, such systems are expensive, put additional restraints on the engine operation and are a sign of incomplete combustion (in all cases except NO_x). The LTC concept is thus introduced to avoid or reduce the formation of emissions prior to after-treatment.

The common feature of the LTC engine concepts is like the name implies to shift the reactive state of the fuel away from high temperature combustion which occurs at undiluted stoichiometric conditions. This can be done by shifting the combustion to occur in zones where formation of emissions is low [11, 12]. Several methods to achieve this have been proposed including homogeneous charge compression ignition (HCCI) [13, 14], reactivity controlled compression ignition (RCCI) [15] and partially premixed combustion (PPC)[16]. One of the first LTC-like production line vehicles is being introduced into the market at the moment of writing through Mazda's SKYACTIV-technology[17], which can utilize direct injection of gasoline with spark assisted ignition of a stratified charge. Whether this type of ICE will gain popularity remains to be seen.

1.2 Objective and scope

This thesis is focused on providing better understanding of the fundamental physics which drive the mixing and combustion in PPC engines. A broad description of the objective is to provide insights to people working with engine design and engine research on how the PPC engine combustion behaves and how it can be modelled. This is done by performing and analysing computational fluid dynamics simulations of the in-cylinder physics. The scope of the work is limited to physical phenomena which occur inside the cylinder or in close proximity to the cylinder. Only a single cylinder is studied at a time.

In LTC engines the combustion process behaves very differently to conventional concepts like SI or Diesel engines. The stratified premixed state of the fuel coupled with compression ignition makes the ignition front propagation an important if not dominating [18] mode

of combustion for such engines. This causes the ignition process to behave unpredictably as the history of turbulent mixing has the strongest effect on the ignition rather than a spark plug like in SI engines or spray induced scalar dissipation as in diesel engines. Thus the main focus of the thesis is on investigating how the turbulence, injection process, ignition process and subsequent modes of combustion interact and how to numerically capture the different physical phenomena which are responsible for the interactions.

A secondary goal is the investigation of how to properly formulate CFD models of PPC engines. The PPC modelling community has inherited some methodology from the more mature Diesel engine modelling community to simplify and speed up calculations of turbulent combustion. This work also investigates the validity of some assumptions which are commonly found in publications of PPC engine simulations. In this study focus is put on generation of initial conditions and the periodic sector assumption.

Chapter 2

Development of reciprocating piston engines

The first part of this chapter gives the reader a quick introduction to the direct injection combustion engine concepts by describing the injection process and subsequent flame structures. The second part of the chapter describes the family of low temperature combustion concepts and defines two characteristic concepts of this kind. The third part of the chapter covers optical research engines, some of the types of measurements which can be obtained from them, and finally some comments on the modelling of such engines.

2.1 Physics in DICI engines

In direct injection engines the fuel enters the cylinder from a high pressure fuel injection system in the form of a liquid spray from a circular or annular orifice. By injecting the liquid fuel at a pressure difference of several hundreds of bars the liquid often cavitates to some extent prior to entering the combustion chamber, causing instabilities in the flow rate. When the liquid fuel then enters the cylinder gas at supersonic velocities, and encounters strong shear forces, the liquid core is further deformed resulting in the shedding of liquid filaments. These filaments then break into droplets that continue to shed, or break into, smaller droplets until full evaporation occurs [19–22].

The process is sensitive to several physical properties which change with the progression of the spray breakup and evaporation. For in-cylinder spray modelling the breakup of small droplets is usually the focus of interests [23]. The shedding of the liquid core and cavitation occurs at time- and velocity-scales which are very different from the rest of the engine combustion process. The treatment of these effects is covered in the modelling chapter.

Depending on the engine concept, after evaporation the fuel has some specific time to

mix with the ambient oxidizer which can consist of pure air or, if exhaust gas recirculation (EGR) is utilized, air diluted with combustion products e.g. CO_2, H_2O. Thus far the described progress is similar in all engines using direct injection.

2.1.1 Structure of conventional diesel combustion

Diesel engines are not counted among the LTC concepts since a majority of the fuel combusts at stoichiometry, but the injection process is similar to PPC and some HCCI engines. In fact PPC combustion at very late injection timings begins to look similar to the combustion structure visbile in conventional diesel combustion (CDC) engines. One of the commonly occurring descriptions of the CDC structure is found in works by Dec et al. [24, 25] as seen in figure 2.1 which shows the progress of liquid evaporation, mixing controlled combustion and other effects unique to CDC, like the high temperature soot formation zone. Because of the high cetane number of diesel fuel the vaporized fuel rich cloud has a short ignition delay time and ignites after a short travel distance which results in a mixing controlled flame structure as seen in the figure. As in most applications in the field of turbulent combustion the real process is not as simple as a single combustion mode and in fact a so called edge flame consisting of auto-ignition, lean and rich premixed flames, and mixing controlled flame occurs at the quasi-steady leading flame front. The late direct injection of diesel engines cause the fuel to be consumed in a mixing controlled combustion mode which operates close to stoichiometry, but a non-negligible part of the rich mixture reacts with oxygen that penetrates the stoichiometry either by turbulent mixing or molecular diffusion. Due to the air entrainment prior to the ignition a lot of air is mixed with the fuel creating a fuel rich premixed gas. Once ignited this fuel rich reacting region is colder than the stoichiometric reaction zone around the spray. This rich premixed flame is a strong source of polycyclic aromatic hydrocarbons (PAH) which are precursors to soot formation. In addition to this the products of the premixed combustion are mixed with the products from the mixing controlled flame which limits oxidation. The stoichiometric reaction zone around the spray at the other hand is a very thin reacting layer due to the immense turbulence induced by the spray momentum. This means that compared to the low temperature combustion concepts described below a relatively small fraction of the fuel is contributing to the heat release at any time. Instead the reactions happen quite fast, resulting in locally high temperatures and NO_x formation levels.

2.2 The low temperature combustion concept

New reciprocating engine concepts have been continuously introduced throughout the history of the ICE, some of which could even fall under the LTC description prior to its

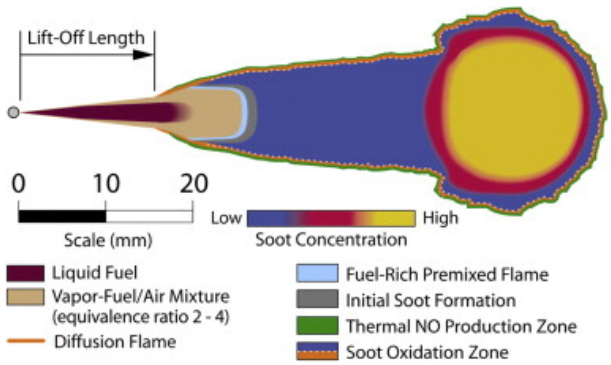

Figure 2.1: The often found schematic description of CDC as stated by Dec et al. Specific cases of late injection PPC show similarities to such a structure.

conception. Engine legislature has always focused on reduced emissions but the new regulation limits were traditionally reached by slight design changes to existing engine concepts, like piston design, boost pressure, injection pressure or the use of EGR. Primary emission reduction targets of legislations have been exhaust fractions of NO_x, CO, UHC and soot.

Even though the concept was first introduced at the end of the 70s [13], it is only during the last few decades that the push towards reduced local emissions and higher efficiency resulted in the first true LTC engine: the homogeneous charge compression ignition (HCCI) engine. The general idea behind the LTC concept is visualized in figure 2.2 which shows at which local values of equivalence ratio and temperature the formation of NO_x and soot tends to occur. The soot formation occurs in rich, low temperature flames while the NO_x formation requires relatively lean mixtures and high temperatures [26–28].

The main idea of LTC is therefore to force the chemical reactions to occur at sufficiently low temperatures, while avoiding mixtures that are too rich [14, 29–31]. Multiple engine concepts with corresponding abbreviations have been proposed to solve this that fall under the LTC description. The concepts often overlap so for simplicity the descriptions used in this thesis are grouped into two main classes; the HCCI and PPC concept.

2.2.1 HCCI engines

The homogeneous charge compression ignition engine concept introduces the charge externally during the intake or at an early phase in the compression stroke so that it mixes into a lean, premixed condition with very low stratification in fuel concentration. This is possible due to the long mixing time which allows the charge to be distributed evenly. As the engine reaches TDC the gas ignites by compression ignition, and the idea is to have a quick and intense heat release in order to maximize the thermodynamic efficiency while avoiding the NO_x and soot formation clouds. Since the mixture is locally lean everywhere

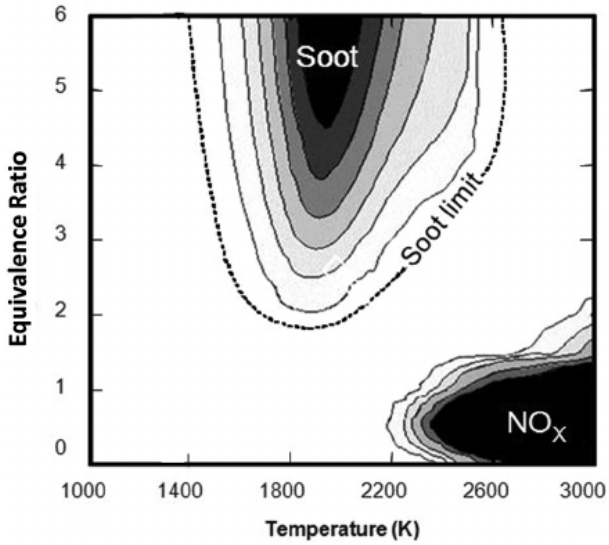

Figure 2.2: The formation regions of soot and nox based on the local equivalence ratio and temperature of the burning mixture [32].

and distributed over the full volume the formation of NO_x is low as is the soot.

Unlike an SI engine the combustion is not driven solely by the propagation of a wrinkled flame front but rather by separate ignition events from compression ignition, even though deflagration can coexist with the ignition front. This makes the combustion less dependent on the level of turbulence at the moment of ignition and can speed up combustion considerably if stratification in ignition delay time τ_i is low. The distribution of τ_i can not be directly controlled since small turbulent fluctuations of τ_i-controlling physical quantities like pressure, mixture fraction and temperature are randomly distributed by the turbulence. For chemical reasons high load cycles tend to burn much faster than the low load cycles and can sometimes deteriorate into knock. Similarly variations in the temperature of piston, liner and cylinder head can affect heat losses during compression which offsets the τ_i, causing knock or misfire depending on ambient temperature and load. In some cases dilution with EGR was introduced to mitigate the difficulty to control the HCCI combustion phasing and enable a wider range of operation.

Even though the fuel is homogeneously distributed in HCCI engines the local values of in-cylinder temperature can vary quite drastically as seen in figure 2.3 [33–36]. The effects of such a stratification in temperature on the combustion characteristics of HCCI varies depending on the chemical kinetic behaviour. In a low load case the mixture is limited by the fuel concentration and will have a small effect on ignition delay time distribution, but in high load cases such a distribution can cause a strong stratification in ignition delay

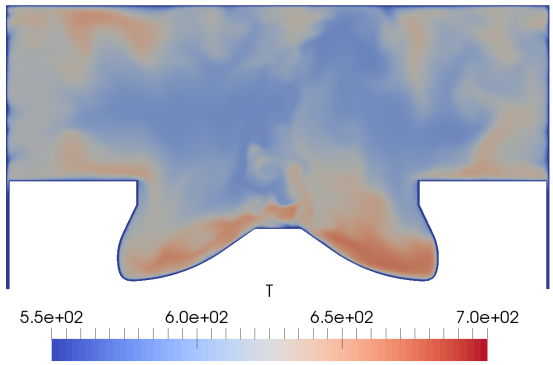

Figure 2.3: A temperature distribution [K] through a central cut of a swirling light duty Volvo I5D cylinder at -54 CA ATDC, prior to injection. The field is obtained from a full cylinder LES run of an optical engine cylinder with initial conditions taken from an open cycle simulation. The range of temperatures show stratification in the order of 100 K. These large temperature variations occur due to the compression of a less severe stratification in the temperature distribution at IVC.

times as well, which affects the combustion speed.

2.2.2 PPC engines

The partially premixed combustion engine concept began as an off-shoot of the development of HCCI engines [37–39] with early injection timings. Due to the control issues of ignition timing in HCCI, experimentation with retarded injection timings introduced a new way of avoiding both soot and NO_x while retaining the high compression ratio and control of the combustion phasing. Early implementations of the PPC concept used high cetane number fuel like Diesel to achieve PPC combustion in order to avoid knocking behaviour at high compression ratios. Early injected gasoline type fuels ignited in a very violent manner in comparison. By stratifying the gasoline charge with split injections [16] the ignition became less violent. Furthermore to enable high compression ratios very high levels of EGR were introduced in order to slow down the reactivity and enable even better control of the ignition [40]. Research continues on how to combine the best reactivity and EGR levels in order to maximise efficiency [41, 42].

The ”PPC engine” is a very broad term and several other LTC engine concepts overlap its operating description, but in this thesis engines which operate according to the principles described below are called PPC engines. In this work the PPC engine description is only used on engines which ignite by means of compression ignition. Figure 2.4 shows one example of how PPC engine combustion can look from a conceptual point of view [43].

The general idea is to inject the fuel at a timings such that, given the chemical behaviour of the fuel at the specific circumstances of the load cycle, a) reactivity occurs in

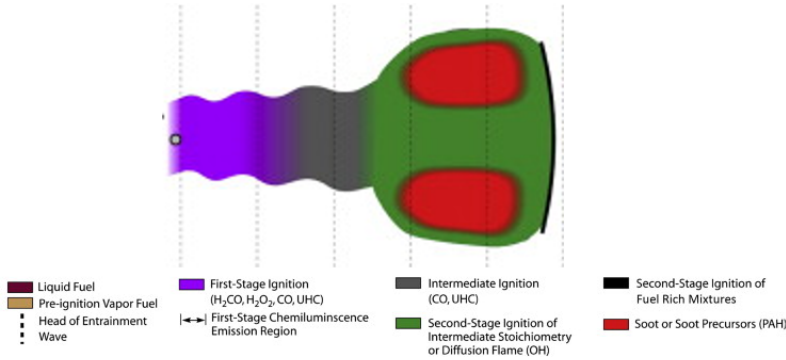

Figure 2.4: A PPC concept image during main combustion reproduced from [43]. The image shows the fuel impingement on the cylinder as seen from the top. The two rich recirculation zones become the main source of soot formation. This type of process occurs when when burning fuels with no oxygen fraction in PPC mode and when injecting the fuel at an intermediate stage.

sufficiently lean environment to avoid soot formation, yet b) fuel concentration must be stratified enough to avoid burning a majority of the fuel in a stoichiometric environment thus avoiding high temperature combustion which generates NO_x. The observant reader notices that the main difference to the description of HCCI is the stratified state of the fuel which indeed is the namesake of the concept. While the work presented in this thesis focuses on the fundamental aspects of mixing and ignition of a single injection experimental work utilizing multiple injections is common [44, 45].

Since this work is numerical in nature the mode of combustion is of particular interest, and the description guarantees that the combustion starts with an ignition front prior to transitioning to some form of deflagration. For the sake of this thesis, an additional criterion can be introduced to separate PPC engine conditions from some of the more premixed conditions in CDC engines; c) If the majority of the heat release occurs during the propagation of an ignition front the engine works in PPC mode. The inclusive and slightly vague definition of PPC engines conveniently ensures that combinations of fuels and engine configurations resulting in similar types of combustion processes collapse on the same class of engine concept. Unfortunately, since most engine simulations are performed using some kind of filtered turbulence formulation, temporal or spatial, and separation between deflagration and ignition front combustion modes requires unfiltered quantities, some ambiguity remains.

Because the stratification in fuel concentration can be achieved in multiple ways there is not a single way to create PPC engine conditions in direct injection compression ignition engines. Injection timings, fuel properties, split injections, swirl ratio, injection pressure and piston design are some control parameters which can be mentioned but no specific combination of parameters guarantees PPC engine-type combustion for all conditions. For

example a low load case with late injection timing for a high cetane fuel can result in mixing controlled CDC, while the same conditions for an alcohol fuel results in a majority of the fuel being burned in a PPC-type premixed ignition front [46].

While there are no production line engines which rely purely on the PPC concept as described here, some manufacturers have introduced engines which utilize similar ideas. "Modulated Kinetics" [47, 48] concept was introduced by the Nissan motor company and relies on earlier injection timings, EGR, high injection pressures and a high swirl in diesel engines. This results in a slightly premixed combustion and avoids soot and NO_x. Unfortunately it comes at the cost of increased UHC and CO emission and a limited operating range. The UNIBUS [49] or uniform bulky combustion system is another diesel modification which utilizes two split injections with very long delay in between. The first injection occurs in the early compression stroke while the other happens at regular diesel timing. The Mazda SKYACTIV [17] technology utilizes early injection timings and EGR as well but avoids the uncertainty with compression ignition by adding a spark plug. Control of ignition timing is assisted by an in-cylinder pressure transducer which helps in knock avoidance and combustion phasing.

2.3 Optical access in reciprocating engines

Production line engine cylinders are made of steel alloys and are closed volumes during the combustion so the only measurable physical gas properties can be obtained at the intake or the exhaust of the cylinder, before or after combustion. In order to obtain information about the actual turbulence chemistry interaction engineers have used optical access for spray and engine studies for a long time [50]. The numerical results in this thesis are compared to the experimental results from three optical engines; the Volvo Cars I5D light duty optical engine[51], the Scania D13 heavy duty optical engine [52] and the Volvo D13 heavy duty optical engine [53]. These are all single cylinder optical engines which utilize a so called Bowditch engine configuration in order to see physical properties from the optical access windows seen in figure 2.5. This enables 2D-pictures of natural luminosity, studies of light scattering and reflection as well as spectroscopic studies.

2.3.1 PIV

Particle image velocimetry is a method which allows the capture and study of fluid flows by deploying small particles into the flow. The travelling paths of the particles can then be reconstructed from images taken at sufficiently small time intervals. The particles themselves need to be of sufficiently small size not to affect the flow. Most combinations of flow, particle size and light wavelength result in signals dominated by Mie- scattering from the particles. PIV can be performed in multiple ways but the 2D planar PIV is the most commonly occurring in engine applications.

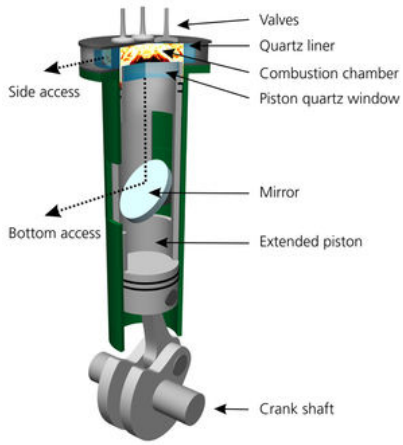

Figure 2.5: The Bowditch engine design which gives access to a side view of the combustion chamber as well as a bottoms up view. If a non-flat piston geometry is used the picture has to be transformed to compensate for refraction effects from the piston surfaces.

2.3.2 Mie scattering

Mie scattering occurs when a plane wave of electromagnetic radiation is scattered inside a spheric object to form specific intensity patterns in the far field. If observed at a constant angle to the plane wave the intensity of scattered light has a monotonous but non-linear dependence on particle diameter and density. Thus Mie scattering images of spray droplets show distributions of liquid droplets but only in a qualitative sense. Generally in optical studies of engines Mie scattering is used in PIV and spray droplet studies.

2.3.3 Spectral analysis

Multiple spectroscopic methods exist to study the chemical composition of a gas mixture or the reactions therein. The simplest way to study reactions is to simply apply thin band-pass filters to images to identify specific reactions which are characteristic for the reactivity in question. In such a case a 2D projection of the volumetric signal is visible on the picture, a so called ”line-of-sight” view. More advanced method with better signal to noise ratios include laser induced fluorescence where a laser pulse reshaped into a plane is used to study the spectroscopic response to the laser induced excitation. This method allows for 2D-pictures of specific chemical components. Combined with other methods this can give useful information on formation and destruction of specific species while the natural chemiluminescence shows where the high temperature reaction zone occurs.

2.3.4 Comment on modelling engines with optical access

Because optical engines are designed for different purposes than efficient power conversion it is not unusual to have high bypass flow between the optical piston and the liner.

This means that the actual mass inside the cylinder might change quite a bit during the combustion, and it's not uncommon to observe pressure traces which correspond to lower compression ratios than the geometric engine compression ratio (or equivalently enormous heat losses, despite no combustion).

Because the optical engine window needs to be as clean as possible it is common to skip multiple cycles between each combustion cycle. This usually means that the inner surfaces of the cylinder have different temperature depending on how the optical engine has been operating. This is further complicated by the piston being made from quartz to enable spectroscopic signals in the near IR spectrum. Quartz has a lower specific heat capacity, and lower conductivity than metal making the cylinder temperature unpredictable.

Finally because the engine is not run continuously as a metal engine the fuel consumption can not be measured over a long period of similar cycle operating conditions. This means that the injected fuel mass of each cycle has to be estimated somehow. Since real IMEPs are hard to measure due to the bypass flow this sometimes leaves the user to model the injected mass based on data like average flow from injector manufacturers, which in turn is given at some reference condition which don't always match experiments, or by using a separate model. In the case of the research presented in this thesis the model proposed by Xu et al. [54] is used as an initial guess. The final fuel mass is determined by iteration and validation of other measurable quantities like pressure trace.

Chapter 3

Theory of flow and combustion in IC engines

This chapter treats how to describe and quantify the physics of reactive fluid motion in direct injection combustion engines. The first part covers the Navier-Stokes equations used in ICEs, the second part gives a brief introduction to the theory of turbulence and turbulent combustion, applied to combustion engines.

3.1 Governing equations of the flow

The equations that govern the motions of viscous fluids are called the Navier-Stokes equations. Strictly speaking the equations are a model for the statistical average motion of dense formations of molecules and so should be mentioned in Chapter 4 together with the other models, but due to the importance and fundamental nature of fluid transport they are treated separately.

While the Navier-Stokes equations can be written in a multitude of ways, the equations below are formulated to describe the physics of in-cylinder gas mixtures in direct injection engines. The equations are thus valid for describing the motion of a Newtonian, sub-sonic, reacting flow with variable density. In order to simplify the equations the material derivative is defined as :

$$\frac{D\phi}{Dt} = \frac{\partial \phi}{\partial t} + u_i \frac{\partial \phi}{\partial x_i} \tag{3.1}$$

Now the conservation of mass in terms of density, can be established through the continuity equation:

$$\frac{\partial \rho}{\partial t} + \frac{\partial \rho u_i}{\partial x_i} = S_\rho \tag{3.2}$$

where ρ is the density and S_ρ is an external source of density, in the present case from the spray. This equation simply states that for an infinitesimal volume following the flow, a change in density can only occur through external introduction of mass.
Following the continuity equation comes the transport equation for momentum:

$$\frac{\partial \rho u_j}{\partial t} + \frac{\partial \rho u_i u_j}{\partial x_i} = -\frac{\partial p}{\partial x_j} + \frac{\partial \tau_{ij}}{\partial x_i} + \rho g_j + S_{u,j} \tag{3.3}$$

where u_j is the velocity in the j-th direction, p is the local pressure field, g_j and $S_{u,j}$ account for external (non gas-flow) sources like gravity and spray and the shear stress tensor τ_{ij} is given below. This equation states how the advective transport is balanced by the pressure, viscous shear and external forces.

The next equation to describe the gas mixture is the transport of chemical species mass fractions Y_k of species k:

$$\frac{\partial \rho Y_k}{\partial t} + \frac{\partial \rho u_i Y_k}{\partial x_i} = -\frac{\partial J_i^k}{\partial x_i} + \dot{\omega}_k + S_{Y,k} \tag{3.4}$$

where J_i^k the diffusive mass flux of the chemical species k in the i-th direction, $\dot{\omega}_k$ is the rate of change due to chemical reactions and $S_{Y,k}$ accounts for the introduction from external sources. As before the equation balances the terms previously mentioned.

Finally to be able to describe the thermodynamic state of the fluid the model must be supplied with two thermodynamic properties, in present case enthalpy and pressure. The pressure distribution in the fluid will be treated at a later stage but the enthalpy is transported according to the equation below:

$$\rho \frac{Dh}{Dt} + \rho \frac{DK}{Dt} - \frac{\partial p}{\partial t} = -\frac{\partial J_i^h}{\partial x_i} + \sum_k h_k^0 \dot{\omega}_k + S_h \tag{3.5}$$

here h is the sensible enthalpy of the gas mixture, K is the total kinetic energy, J_i^h is the conductive heat flux in direction i, h_k^0 is the formation enthalpy of species k and S_h is an external source term. In this equation the balance between thermal and mechanical energy of an infinitesimal volume following the flow is described by the contributing terms; conductivity, heat release and external sources.

The gas mixture is described by its constituents - the chemical species mass fractions. The thermodynamic pressure of the mixture depends on the temperature by the ideal gas law:

$$p = \rho R_u T \sum_{k=1}^{N_s} \frac{Y_k}{W_k} \tag{3.6}$$

where W_k is the molecular weight of specie k, R_u is the universal gas constant, T is the temperature and N_s is the number of species. The shear stress in the fluid is assumed to follow that of an ideal Newtonian fluid:

$$\tau_{ij} = \mu \left(\frac{\partial u_i}{\partial x_j} + \frac{\partial u_j}{\partial x_i} - \frac{2}{3} \frac{\partial u_k}{\partial x_k} \delta_{ij} \right) \tag{3.7}$$

Here the δ_{ij} is the Kronecker delta function and μ is the dynamic viscosity. The molecular fluxes are described using Fick's law for the diffusive mass flux and Fourier's law for conductive heat flux.

$$J_i^k = -\rho D \frac{\partial Y_k}{\partial x_i} \tag{3.8}$$

$$J_i^h = -\rho \alpha \frac{\partial h}{\partial x_i} \tag{3.9}$$

This concludes the description of the governing equations of the flow.

3.1.1 Comment on the deterministic nature of Navier-Stokes

Because the Navier-Stokes equations describe the motion of a continuous field, detailed information about the state of molecular properties is lost and is only represented through the average quantities described in the section above. For this reason, even before applying methods to solving such equations, the equations are only true in a statistical sense - meaning that every quantity can only be represented as a continuum average. This means that even though a specific flow situation always progresses the same (deterministic) way according to the Navier-Stokes equations, the resulting state of such a simulation is calculated from the interaction of continuum-average quantities and will therefore only agree in a statistical sense with experiments.

3.2 Governing equations of the chemistry

The chemical change rate $\dot{\omega}_k$ for species k is expressed as a density change rate ($kg/m^3/s$) and is related to a change in molar concentration c_k as shown below.

$$\dot{\omega}_k = \frac{dc_k}{dt} W_k \tag{3.10}$$

The change in molar concentration for all species due to chemical reactions can be expressed in the following series:

$$\frac{dc_k}{dt} = \sum_{r=1}^{R} k_r \left(v_{rk}^{(p)} - v_{rk}^{(e)} \right) \prod_{k=1}^{N_s} c_k^{v_{rk}^{(e)}} \tag{3.11}$$

where the sum loops over all reactions $r = \{1..R\}$, and the product over all species contributing to the species in question $k = \{1..N_s\}$. The $v_{rk}^{(p)}$ and $v_{rk}^{(e)}$ are stoichiometric coefficients for products and reactants, k_r is a reaction coefficient calculated from the Arrhenius formula stated below.

$$k_r = AT^b e^{-\frac{E_a}{R_u T}} \tag{3.12}$$

The pre-exponential factor A is determined empirically, as is the temperature dependence b. E_a is the activation energy for the reaction. This closes the section covering governing equations of the chemistry.

3.3 Description of turbulence

3.3.1 Energy spectrum

Andrew F. Richardsson proposed in the 1920s that the swirling structures seen in the turbulent flows of viscous fluids were all part of a turbulent cascade where new smaller structures are formed from large ones. This cascade continues to form new smaller members until the structures are so small that the viscous forces of the flow cannot be overcome, see figure 3.1. The largest scales of motion form the integral range where most of the energy is contained. These usually contain or siphon off some geometrically constrained flow. These in turn shed eddies in the inertial sub-range which holds the widest range of wave-numbers. The range containing the smallest scales is called the viscous sub-range.

This theory of the turbulent cascade has been generally accepted and completed with other phenomena by multiple contributors. One of the most prominent among these was the Russian mathematician Andrei Kolmogorov who presented three hypotheses regarding turbulence:

- For some sufficiently high Reynolds number, the smallest scales of turbulence have no particular orientation and can be considered isotropic, in a statistical sense. This is called Kolmogorov's hypothesis of local isotropy
- At sufficiently high Reynolds numbers, since the smallest scales have lost their original orientation they behave very similarly and depend only on viscosity ν and the rate of turbulent dissipation of energy ϵ. This is called Kolmogorov's first similarity hypothesis
- Kolmogorov's second similarity hypothesis is based on the fact that the intermediate scales cover a large number of wave-numbers and are not as dependent on viscosity as the viscous sub-range. Thus the average scale is determined uniquely by ϵ, independent of ν.

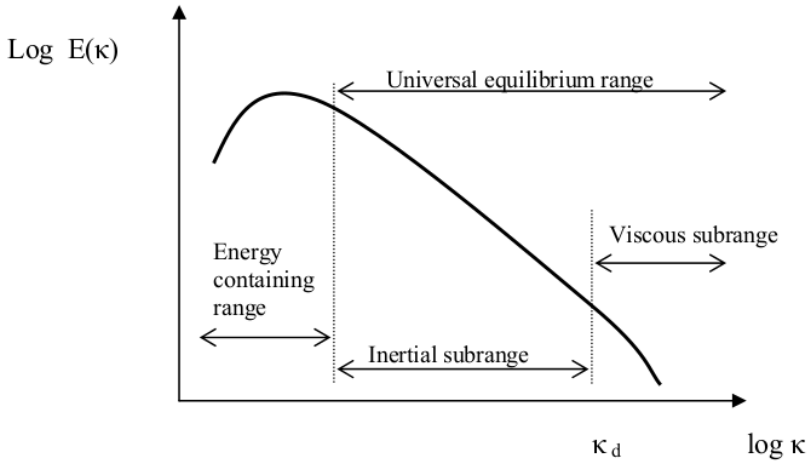

Figure 3.1: An idealized image of the energy cascade showing the inertial and viscous sub-range. The horizontal axis shows the wave number and the vertical axis shows the kinetic energy. The near-linear behaviour in the inertial sub-range can be proven to hold a -5/3 slope by dimensional analysis.

Dimensional analysis regarding the first similarity hypothesis can show that the smallest length scales can be estimated as

$$\eta = \left(\frac{\nu^3}{\epsilon}\right)^{1/4} \tag{3.13}$$

which today is known as the Kolmogorov length scale. The size of such a scale is drastically smaller than the integral scale which makes it very arduous to simulate. Kolmogorov's second similarity hypothesis explains why the inertial sub-range behaves in such a predictable way. The viscous sub-range and inertial sub-range are often together called the universal equilibrium range in reference to the fact that they adapt to the energy transfer rate of the largest eddies. This is possible because the universal equilibrium range decays and forms so much faster than the integral range, which in turn means that the whole energy cascade is determined by the integral scales. This makes sense since there would otherwise be a build-up of energy at some other wave-number which is limiting the cascade.

3.3.2 Characteristics of turbulence

While turbulent flow has no formal definition, some characteristic features are commonly attributed to it [55].

- Irregular - The observable turbulent structures (eddies) in turbulent flows have certain scales, or properties, like a length scale and velocity scale. Turbulent flows are made up from structures from a range of such scales and the distribution of these is irregular.

- Diffusive - Turbulent flows are diffusive and turbulence itself acts as a diffusivity enhancer (and is in fact often modelled like one). The increased mass transport from small scales which are often oriented isotropically is similar in many ways to the Brownian motion which is the underlying mechanism of diffusivity.
- High Reynolds number - A high Reynolds number is required to obtain a transition to a turbulent flow. The transition Reynolds number depends on the flow case but can range from a few thousand and upward.
- Three dimensions - Turbulence is a three dimensional phenomenon. While 2D-turbulence can be obtained in simulations such system always deposit the energy in the integral range, requiring some artificial way of draining the large scale motions. Without three dimensions the statistics of turbulence become altered.
- Dissipative - Turbulent structures lose their energy to smaller structures continuously until the viscous forces dissipate it to heat.
- Continuous - All flow structures are larger than the molecular scales and in fact continuum is a requirement for the energy cascade to exist.

3.3.3 Non-dimensional numbers in turbulent flows

Since turbulence behaves randomly and is a product of transient processes it's hard to measure classical observables in a meaningful way. Momentum magnitude and direction changes rapidly due to the inherent nature of turbulence. When looking at the behaviour of a specific range of scales in the cascade it is very comfortable to represent such a range by the characteristic scale of the range either in length, time or velocity scale form. Such scales can be defined for the whole cascade, ranging from the largest integral scales in length, time and velocity, l_0, τ_0, u_0, to the smallest Kolmogorov scales in the same dimensions η, τ_η, u_η. Based on such scales key characteristic dimensionless numbers can be used to describe important aspects of the flow in a short yet meaningful way. In descriptions of turbulent flows the most commonly found dimensionless number is the turbulent Reynolds number, often shortened as Re_0:

$$Re_0 = \frac{u_0 \cdot l_0}{\nu} \tag{3.14}$$

where l_0 and u_0 are the characteristic length scale, the velocity scale of the integral range and ν is the kinematic viscosity scale representative of the flow. This turbulent Reynolds number describes the ratio of momentum transport to viscous transport of the largest most energetic (integral) scales, but the Reynolds number can be used to describe any scale in the cascade. As the scale size decreases so will the Reynolds number until the Kolmogorov length scale which has $Re_\eta = 1$. In fact dimensional analysis can show that the Kolmogorov scales are related to their integral versions as a function of the integral Reynolds

number. In reciprocating engines, during injection, it is not uncommon to find integral Reynolds numbers reaching values above 10^6, implying that the range of scales present in such an engine is very wide.

Similarly to how a characteristic viscosity is used to obtain the Reynolds number another non-dimensional value called the Schmidt, Sc, number describes the ratio of diffusive to viscous transport:

$$Sc = \frac{\nu}{D} \tag{3.15}$$

here D is the characteristic molecular diffusivity as seen in equation 3.8. It should be noted here that different chemical species can have different rates of diffusivity, depending on molecular properties. In particular any chemical process oriented around the diffusion of hydrogen needs to take variable diffusivity into account, but in the work presented in this thesis all species are considered to have the same diffusivity. This prompts the introduction of another dimensionless number called the Lewis number, Le, which is defined as:

$$Le = \frac{\alpha}{D} \tag{3.16}$$

where α is the heat conductivity. All simulations described in the thesis are assumed to have unity Lewis number, equalling the thermal conductivity to the diffusivity in all species. To close the circle the Prandtl Pr number is introduced:

$$Pr = \frac{\nu}{\alpha} \tag{3.17}$$

If the viscosity of a fluid is known the Sc and Pr numbers can be used to obtain values of D and α for equations 3.8 and 3.9 respectively.

3.4 Swirl and tumble

To improve mixing in combustion engines a so called swirl structure is often formed during the gas exchange process. This swirl effect comes from the design of the intake runners and the valve timings, which force the intake air to form a rotating flow in the cylinder as seen in figure 3.2. The swirl number in an engine is defined as the ratio between the rotational frequency of the gas and the frequency in the piston motion. A representative rotational frequency of the gas is estimated by that of a solid body equivalent containing the same angular momentum, relative to its center of mass. In a cylindrical reference frame oriented in the engine cylinder direction with an origin in the center of gas mass the axial angular momentum (along the piston motion) is given by:

$$L_z = \int_m x_r \cdot u_\phi \cdot dm \tag{3.18}$$

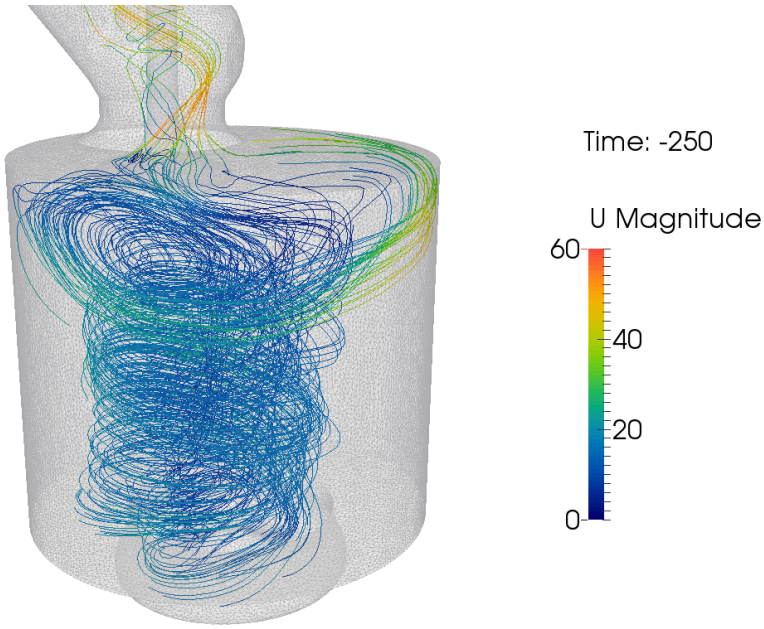

Figure 3.2: Streamlines of the Reynolds average flow in a cylinder during gas exchange. The swirl rotating direction is not perfectly oriented with the piston axis and in fact the direction keeps rotating around the axis.

where x_r is the radial distance from the center of mass and u_ϕ is the tangential velocity component, rotating around the center of mass. The integral sums over all the gas mass in the cylinder. Calculating the moment of inertia:

$$I_{zz} = \int_m {x_r}^2 \cdot dm \tag{3.19}$$

one can obtain the rotational frequency of a solid body equivalent

$$\omega_z = \frac{L_z}{I_{zz}} \tag{3.20}$$

which in turn can be compared to the piston rotational frequency to give the swirl number:

$$S_n = \frac{\omega_z}{rpm/60 \cdot 2\pi} \tag{3.21}$$

where the rpm is the engine speed in revolutions per minute. A very similar derivation of the tumble number can be obtained by projecting the angular momentum vector perpendicularly to the axis and calculating the moment of inertia for the rotation perpendicular to the axis as well.

3.5 Combustion in IC engines

Turbulent combustion is a very large subject encompassing phenomena seen in candles, space rocket engines, explosions and stars undergoing a supernovae transformation. The theory presented here will be a cutout of the relevant phenomena usually found in combustion engines.

3.5.1 Scales and characteristics in combustion

Similar to how turbulent flow can be described using characteristic scales of turbulence in section 3.3.3 the turbulent combustion can be described here using similar methods. The most commonly used representative scale of the chemistry is the turbulent time-scale, commonly written as τ_c. Such a time-scale is often compared to turbulent time scales of various kinds yielding non-dimensional numbers that describe certain aspects of the flow [56]. The ratio between the integral turbulent time scale and the chemical time scale is called the Damköhler number:

$$Da = \frac{\tau_0}{\tau_c} \tag{3.22}$$

While the description Damköhler number can be used for the ratio of any turbulent scale to chemistry the most common meaning is that of the integral timescale.

The ratio of the chemistry time scale to the Kolmogorov time scale is called the Karlovitz number and can be particularly important in the study of premixed flames.

$$Ka = \frac{\tau_c}{\tau_\eta} \tag{3.23}$$

The fraction of mass which originates from the fuel is a very useful quantity, described by the mixture fraction:

$$Z = \frac{m_{fuel}}{m_{mixture}} \tag{3.24}$$

For all the work presented in this thesis mass which which originates from the fuel m_{fuel} excludes combustion products from previous engine cycles.

3.5.2 Modes of combustion

A combustion mode is a grouping of situations in which the high temperature reaction of fuel and oxidizer undergo similar physical processes. In ICEs the most common modes of combustion are the premixed deflagration, non-premixed flame wave and the ignition front wave.

Premixed deflagration wave

The typical description of premixed deflagration wave depicts a reacting flame front propagating through an unburned but premixed mixture of fuel and oxidizer, leaving behind it a hot low-density zone of combustion products. Depending on the relative difference in scales of turbulence to the reaction zone thickness (often described by the Ka number), the flame can be completely unaffected by turbulent transport as is the case in laminar flamelet, or can reach increasing degrees of flame-turbulence interaction, depending on the relative scale size between the turbulence and flame thickness, as described in the Borghi-diagram [57]. In the case of reciprocating engines the quantities that classify premixed flames like laminar flame speed are hard to obtain due to the extraordinary high pressures at which the combustion occurs, and so determination of flame regime becomes very hard. Generally in the presented PPC papers the premixed flame is in a mixed mode with an ignition front. In such a case the deflagration occurs in piecewise segments where gradient in ignition delay time is too high for the ignition front to propagate [58]. All in all not much can be said about premixed flames in PPC combustion engines except that they exist and are a vital part of the reaction front propagation process.

Non-premixed flame

Non-premixed flame is sometimes called a diffusion flame or mixing controlled flame. As the name implies non-premixed flames happen in the bounding gas interface around mixtures where no fuel or oxidizer exists, where fresh reactants must be transported through the interface in order to burn. Without any help from turbulent transport the reactants must rely only on diffusion to reach the reaction zone. If the time-scale of mixing is much higher than the time-scale of chemistry (i.e. if the Damköhler number is very large) the fuel and oxidizer burn almost as soon as they coexist (the idealised so called Burke-Schumann flame sheet model). Even though high turbulence non-premixed flames approach this solution the fuel and oxidizer always has some overlap, which complicates modelling because the relative balance between the chemistry and the scalar dissipation rate determines the physical process.

In Diesel engines, due to the fact that fuel is injected in a high velocity fuel spray the mixing layer formed by the shear stress around the spray generates high turbulence which greatly enhances the mixing process. In PPC engines the non-premixed state of combustion can occur after the premixed combustion has consumed all the available oxygen present in a fuel cloud. At this point a reaction zone will form around the stoichiometric mixture fraction Z_{st}, where mixing controlled combustion will occur. Depending on fuel type the spray may or may not be active after premixed combustion is complete - however since this thesis treats combustion in fuels which are comparable to gasoline, conditions are chosen in such a way that most of the spray induced momentum has dissipated at the start of combustion. Unlike the diesel case there are no strong shear forces left around the fuel cloud, causing a

much slower combustion event than the mixing controlled flame in a Diesel engine. Fortunately more dissipation of turbulent energy means that the fuel has experienced mixing already - usually leaving a relatively small fuel mass to burn in this slow, product-diluted, non-premixed state of combustion.

Ignition front

The ignition front is a premixed combustion mode but is different from the deflagrating combustion modes since it isn't dependent on transport phenomena at the moment of combustion. This is because the ignition front in reality is a set of separate ignition events which happen to occur continuously (because there are no discontinuous distributions in subsonic fluids). For this reason there is no mechanical limit to the reaction front "propagation speed" and it is independent on the characteristics of the flow. However, these ignition events are distributed due to physical properties like temperature, mixture fraction and pressure which, in a turbulent flow, is hard to control.

If the ignition delay time $\tau_i(Z, T, p)$ is defined as the time left for a mixture to ignite in a constant volume reactor at specific conditions then the reaction front displacement speed S_d can be defined as proportional to the inverse of the gradient of ignition delay time, as shown by Zel'Dovich [59],

$$S_d = C \cdot (\nabla \tau_i)^{-1} \tag{3.25}$$

However this is only valid if the propagation of the ignition front happens at a rate which is much higher than the flow velocity, i.e. if the ignition front Karlovitz number is very high. If this is not the case the flow velocity will catch up to the ignition front and perturb it, starting a deflagration of the premixed fuel/oxidizer mixture. Such mixed mode combustion is commonly found in PPC engines where the distribution of ignition delay times is often a non-monotonous function in space. The interaction between ignition front and deflagration combustion mode in stratified premixed mixtures has been reported in numerous direct numerical simulation papers [34, 60–65].

Chapter 4

CFD models for IC engines

4.1 Numeric discretization of the Navier-Stokes equations

No analytic method for finding general solutions to the Navier-Stokes equations exists, but numerical approximations can be obtained based on a discretized formulation of the equations. In this thesis all numerical simulations are performed in the OpenFOAM framework which utilizes an implicit finite volume approach to approximate solutions to the Navier-Stokes equations. For brevity these approximated solutions are simply referred to as solutions.

In order to obtain a solution, the field in question is divided into small volumes called cells, and the progression in time of any solution is performed in discrete time steps. The governing equations of chapter 3 are implemented at each cell interface and for each cell and transported quantity the balance of transports and sources to and from the cell is solved at each discrete time. As there is a co-dependence between cell solution values due to conservation of scalars such a solution is solved implicitly for all cells at once in a big matrix in an iterative manner so as to minimize solution error residuals.

4.1.1 Temporal and spatial discretization schemes

In order to obtain values for the spatial and temporal derivatives seen in the governing equations of chapter 3 between the cells, so called discretization schemes must be applied to the field in question. Since the fields are discretized the value of the derivatives is an estimation of the real, continuous, derivatives. There are multiple ways to estimate derivatives and the best choice depends on the required accuracy, speed or stability of the simulation. Generally speaking the accuracy of a discretization scheme comes at a cost of stability or speed, usually both. Accuracy in discretization schemes is measured in the number of Taylor expansion terms of the real, continuous derivative which the discretization scheme can follow.

For spatial discretization of LES studies presented in this thesis the Gauss linear interpolation scheme is used. It is second order accurate, has a low diffusivity for hexahedral mesh and is relatively fast. It utilizes the Gauss divergence theorem to calculate the divergence of a field between points N and P:

$$\int_V \nabla\phi dv = \oint_{\partial V} \phi\bar{n}ds = \sum_f \bar{s}_f\phi_f \tag{4.1}$$

where

$$\phi_f = f_x\phi_P + (1 - f_x)\,\phi_N \tag{4.2}$$

and the f_x denotes the linear interpolation parameter between N and P.

For temporal discretization in LES the second order accurate backwards discretization scheme was used:

$$\frac{\partial\phi}{\partial t} = \frac{1}{\Delta t}\left(\frac{3}{2}\phi - 2\phi^0 + \frac{1}{2}\phi^{00}\right) \tag{4.3}$$

In essence accurate discretization schemes are a way of compensating for the fact that the discretization is not perfect (infinite) in time and space. Of course better accuracy is always possible by simply increasing the mesh or time-step resolution, but it's not always the most cost-efficient way of reaching an accurate solution.

4.1.2 Mesh in IC engines

Engines, like most applications in CFD modelling, use real non-ideal geometries that can't be approximated by simple boxes or other basic geometric shapes. Hexahedral meshes give a very low diffusivity to the Since engine geometry has a cylindrical symmetry the O-grid technique is well suited for meshing the volume. In order to obtain high accuracy in critical regions such as around the spray and impingement positions local refinement is applied. General mesh size target is 0.4 mm for base mesh and 0.2 mm for refined regions in large eddy simulations. While studies of spray characteristics like liquid and vapour penetration for this mesh size are not perfectly converged, a sufficiently stagnant mesh dependency is observed. For Reynolds average simulations an average mesh sie of 0.8 mm was used without refinement. All simulations presented in the thesis utilize unstructured hexahedral mesh for the bulk flow structures. Irregular occurrence of tetrahedral cells can sometimes be found close to complicated boundaries or at the boundaries surrounding refinement volumes.

Mesh of in-cylinder geometries can be complex and contain many details which have little to no impact on flow. In the work presented here all closed cycle simulations have simplified flat cylinder heads with no valve geometry visible. Similarly the squish region of the cylinder is perfectly flat with no valve pockets.

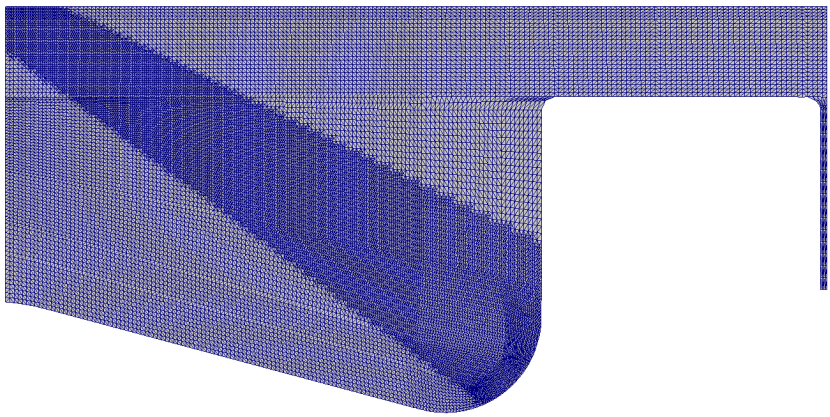

Figure 4.1: A cut through the center of a 72° cylinder sector mesh with a cone shaped refinement around the spray region. This mesh contains 1.4 million cells and is used for with LES.

4.1.3 Boundary displacement

Because of the nature of combustion engines the simulated domain is constantly moving in some way. There are multiple ways to treat deformation of the domain in CFD, including mesh deformation, cell layer addition, immersed boundary techniques or even particle based solvers. The matter presented in this thesis utilizes the mesh compression technique[66–68].

The discretized equations that govern the transport are formulated for set boundaries. When a cell face moves through a flow it will, from a Lagrangian point of reference, experience a flux in the opposite direction to the movement. To maintain scalar conservation in the equations a treatment for this flux has to be included in each cell. For the continuity equation this becomes:

$$\frac{\partial \rho}{\partial t} + \frac{\partial \rho \left(u_i - u_{b,i} \right)}{\partial x_i} = S_\rho \tag{4.4}$$

where $u_{b,i}$ is the boundary movement in the "i"-direction [69]. The second term in the parenthesis of the advective term becomes similar for all transported quantities and is usually represented by a common mass flux ϕ_b in all transport equations, but is left out for brevity in the equations presented in this thesis.

In the case of the axial motion of the piston, uniform compression of the volume above the piston is implemented in the OpenFOAM standard engine solvers. Since it's easy to orient

the hexahedral mesh so that it's compressed in a non-skewing direction the only problem occurs when the aspect ratio of the compressed cells is too high. The volume can change by a factor of 10 during a simulation, and unless the simulation only studies phenomena very close to TDC or BDC, the aspect ratios usually become problematic at some points. By mapping the fields to a new mesh and continuing the simulation this is circumvented and the simulation can continue until deformation reaches such a point that a new mesh change is required.

In some cases the volume deformation does not occur in a single direction, for example in the case of tilted valve motion during gas exchange. For such a case the mesh is allowed to deform dynamically based on the movement of the boundaries. A separate Poisson-equation is solved for node positions at every time-step in the mesh:

$$\frac{\partial}{\partial x_i}\left(\gamma\frac{\partial u_{node,i}}{\partial x_i}\right) = S_{b,i} \tag{4.5}$$

where $u_{node,i}$ is a displacement speed for the node in the current time step and γ is a diffusivity parameter for node movement. $S_{b,i}$ can represent "forces" acting upon the node due to closeness to deforming boundaries. This means that the nodes closest to the boundary will be more prone to movement than bulk nodes. After node displacement is calculated based on old coordinates the mesh is deformed according to

$$x^{new}_{node,i} = x^{old}_{node,i} + u_{node,i} \cdot \Delta t \tag{4.6}$$

and the fields are mapped to the new mesh. It is not necessary to include this process in every time-step if the deforming motion is much slower than the progression of the solution.

4.2 Treatment of turbulence

While the Navier-Stokes equations can describe all scales of turbulence, the computational time required to describe the effect from small scales in a resolved manner is very high. Nevertheless it is possible to calculate fully resolved momentum for limited volumes or very low turbulent intensities. For larger volumes and/or highly turbulent flows the computational cost quickly increases.

To reduce the computational cost of simulating flow with small scales, it is possible to treat certain aspects of the effects of the smallest scales outside the set of transport equations. One way to achieve this is to filter out some part of the scales applying a mathematical filter. This is done by convolution of the Navier-Stokes equations, resulting fields filtered with a specific filter kernel. The equations will transport filtered versions of the original quantities instead:

$$\bar{\phi} = \int_{\Omega} G \cdot \phi \cdot dr \tag{4.7}$$

where G is a filter kernel, and ϕ is unfiltered field and the $\bar{\phi}$ is the filtered field.

The selection of filter G can be done in multiple ways depending on which wavelengths are targeted and how the numerical implementation is performed. As such the actual filtering represents the loss of information due to unresolved scales and numerics. In order for the discretized filtered equations to approximate filtered solutions to Navier-Stokes equations the filter kernel G has to fulfil certain qualities such as scalar conservation, linearity and commutation with derivatives. Since the filtered solution rarely is independent on what was filtered away, such effects need to be somehow calculated and included and are referred to as turbulence models. If the turbulence model works properly it will compensate for the lost effects from the unresolved wave-numbers and and the resolved fields continue to be an accurate filtered solution to the Navier-Stokes equations. The unresolved quantities are defined as:

$$\phi' = \phi - \bar{\phi} \tag{4.8}$$

4.2.1 Direct numerical simulation

Direct numerical simulations (DNS) resolve the full kinetic energy spectrum without any simplifications of the turbulence description. While exact academic requirement to refer to a simulation as a DNS is debatable, the smallest possible energetic scales, the Kolmogorov scales, must be sufficiently resolved in both time and space. This means that the grid must be discretized in space so that the Kolmogorov length-scale η is mesh independent. The filter kernel in this case is supposed to be sufficiently close to a Dirac delta function.

Similarly the time discretization must be small enough to capture the dynamic effects of the Kolmogorov scale, meaning that the simulation time step must be a sufficiently small fraction of the Kolmogorov τ_η.

As previously stated in section 3.1.1, even if such detail is accomplished the resulting solution can not be expected to replicate the physical process in a fully deterministic way, since the interaction of continuum average quantities can only represent the molecular interactions in a statistical sense.

4.2.2 Large eddy simulations

Using the LES turbulence formulation means that the filtering is based on the size of scales, where the filter size is based on which scales the grid cannot resolve. Depending on how the

filter is chosen (i.e. the implicit result of how numeric options such as mesh size, quality and discretization are selected), the contribution to the solution from a certain wave-number and upward the will be increasingly attenuated. This cut-off is not sharp but rather acts over a range of scales.

For all simulations using the LES formulation in this thesis the static single equation transported sub-grid turbulence model is used [70]. Unresolved scales are represented in the form of a transported scalar value of unresolved kinetic energy, k_{sgs}. The advective effects of this unresolved kinetic energy acts on the other transported quantities by means of gradient diffusion through the so called turbulent viscosity assumption. This means that any anisotropic direction the unresolved turbulence has is disregarded in favour of a simplified viscous or diffusive transport. The advection from unresolved scales presented as a turbulent viscosity ν_{sgs} is calculated accordingly:

$$\nu_{sgs} = C_k \sqrt{k_{sgs}} \Delta \tag{4.9}$$

Here C_k is 0.094 and Δ is the filter cut-off length, estimated by the characteristic cell scale:

$$\Delta = (dx \cdot dy \cdot dz)^{1/3} \tag{4.10}$$

The transport equations for the filtered quantities follow below. The first equation is the continuity equation:

$$\frac{\partial \bar{\rho}}{\partial t} + \frac{\partial \tilde{u}_i \bar{\rho}}{\partial x_i} = S_\rho \tag{4.11}$$

the bar above the $\bar{\rho}$ denotes the spatially filtered quantity and $\tilde{u_i}$ denotes the Favre-filtered velocity. Filtered source terms from spray modelling are present on the far right of all equations. The momentum transport equation follows:

$$\bar{\rho}\frac{D\tilde{u}_j}{Dt} = \frac{\partial}{\partial x_i}\left(\bar{\rho}\left(\nu + \nu_{sgs}\right)\left(\frac{\partial \tilde{u_j}}{\partial x_i} + \frac{\partial \tilde{u_i}}{\partial x_j} - \delta_{ij}\frac{2}{3}\frac{\partial \tilde{u}_k}{\partial x_k}\right)\right) - \frac{\partial \bar{p}}{\partial x_j} + S_{u,j} \tag{4.12}$$

Here the tilde in $\tilde{u}_j$ denotes the Favre-filtered quantity, meaning that the quantity is weighted by density in the spatial filtering. The diffusive term includes both molecular diffusivity and advection from small scale effects acting through the turbulent viscosity. Strictly speaking the molecular diffusivity ν is a filtered quantity but written without the bar. The filtered energy equation follows:

$$\bar{\rho}\frac{D\tilde{h}}{Dt} + \bar{\rho}\frac{D\tilde{K}}{Dt} - \frac{\partial \bar{p}}{\partial t} = \frac{\partial}{\partial x_i}\left(\bar{\rho}\frac{\nu + \nu_{sgs}}{Pr}\frac{\partial \tilde{h}}{\partial x_i}\right) + \sum_l \dot{\tilde{\omega}}_l \bar{\rho} h_l^0 + S_h \tag{4.13}$$

where the $\dot{\omega}_l$ is dependent on the choice of combustion model and h_l^0 is the formation enthalpy of species l. The Prandtl number Pr is exactly 1 for all simulations presented. Species are transported according to:

$$\bar{\rho}\frac{D\tilde{Y}_l}{Dt} = \frac{\partial}{\partial x_i}\left(\bar{\rho}\frac{\nu + \nu_{sgs}}{Sc_l}\frac{\partial \tilde{Y}_l}{\partial x_i}\right) + \dot{\bar{\omega}}_l + S_l \tag{4.14}$$

Where the Schmidt number Sc_l is assumed to be exactly 1 for all species. The transport of the unresolved kinetic energy k_{sgs} follows:

$$\bar{\rho}\frac{Dk_{sgs}}{Dt} = \frac{\partial}{\partial x_i}\left(\bar{\rho}\left(\nu + \nu_{sgs}\right)\frac{\partial k_{sgs}}{\partial x_i}\right) + \bar{\rho}\tau_{ij}^{sgs}\tilde{S}_{ij} - \frac{C_\epsilon k_{sgs}^{3/2}}{\Delta} \tag{4.15}$$

where coefficient C_ϵ is 1.048. This concludes the LES formulation.

LES simulations are often used in engines to study cycle-to-cycle variations which can't be observed in RAS or to investigate how more resolved flow interacts with chemistry [71–74]. In the current work the main motivation for the use of the LES turbulence model is to better capture non-isotropic mixing behaviour [36] and to be able to represent scalar stratification due to large scales [18].

It should be noted that the interpretation of what an LES field actually represents is a bit complicated. The resolved scales represent a deterministic instance of a flow and are interacting with unresolved scales which in turn are represented in an average sense. This means that prior to starting a simulation the model requires some knowledge about how large a numerical grid can be allowed, in order to represent the unresolved scales properly. This incompleteness of the LES model is discussed in detail by Pope in [75].

4.2.3 Reynolds average simulations

The RAS turbulence model is based on the famous Reynolds decomposition applied on a field ϕ

$$\phi = \bar{\phi} + \phi' \tag{4.16}$$

the $\bar{\phi}$ denotes the time/ensemble average value of the field and the ϕ' denote the turbulent fluctuations around said average value. The quantity ϕ' is defined in such a way that its time average is always exactly 0. The Reynolds decomposition can be applied in a true time averaged sense where fluctuating value of ϕ over an infinite time averages to $\bar{\phi}$, or as a cyclic ensemble average. The first interpretation is used for steady state flow descriptions and the latter interpretation for an infinite series of unsteady (time dependent) processes. The unsteady solution $\phi(t)$ is then part of an infinitely repeating process with duration $\mathrm{t} = \{\mathrm{t}_0..\mathrm{t}_1\}$ and at time t of the infinite ensemble of events the average value is $\bar{\phi}(t)$. As

reciprocating piston engine cycles are repeating processes the unsteady formulation is usually a good approach in such applications.

Since RAS employs temporal filtering equation 4.7 can no longer be used to describe the information loss and the filtering will not be directly coupled to the size of the grid as in the LES model. Instead the filter is based on a separate model, describing the state of the turbulence in the solution. The effect of the turbulence on the average quantities act through viscous forces as in the LES case through a turbulent viscosity defined as:

$$\nu_t = C_\nu \frac{k^2}{\epsilon} \tag{4.17}$$

where C_ν is a dimensionless coefficient with a value of 0.09. The turbulent kinetic energy or k is representing the kinetic energy in which is not part of the average kinetic energy and the turbulent dissipation rate ϵ describes how fast the turbulent kinetic energy dissipates. Both quantities are transported according to the equations found below. Together this description forms the $k-\epsilon$ turbulence model often used to describe turbulent flows in RAS.

The RAS formulations of mass continuity, momentum, energy and species transport are found below in equations 4.18-4.21. For the RAS equations the overbar denotes Reynolds filter and tilde denotes Favre filtering (density weighted) in the Reynolds sense. All the terms called S on the RHS are source terms due to LPT (filtered).

$$\frac{\partial \bar{\rho}}{\partial t} + \frac{\partial \bar{\rho}\tilde{u}_i}{\partial x_i} = S_\rho \tag{4.18}$$

$$\bar{\rho}\frac{D\tilde{u}_j}{Dt} = -\frac{\partial \bar{p}}{\partial x_j} + \frac{\partial}{\partial x_i}\left(\bar{\rho}\left(\nu+\nu_t\right)\left(\frac{\partial \tilde{u}_j}{\partial x_i} + \frac{\partial \tilde{u}_i}{\partial x_j} - \delta_{i,j}\frac{2}{3}\frac{\partial \tilde{u}_k}{\partial x_k}\right) - \frac{2}{3}\bar{\rho}k\delta_{i,j}\right) + S_{u,j} \tag{4.19}$$

$$\bar{\rho}\frac{D\tilde{h}}{Dt} + \bar{\rho}\frac{D\tilde{K}}{Dt} - \frac{\partial \bar{p}}{\partial t} = \frac{\partial}{\partial x_i}\left(\bar{\rho}\frac{(\nu+\nu_t)}{Pr}\frac{\partial \tilde{h}}{\partial x_i}\right) + \sum_l \dot{\tilde{\omega}}_l \bar{\rho} h_l^0 + S_h \tag{4.20}$$

$$\bar{\rho}\frac{D\tilde{Y}_l}{Dt} = \frac{\partial}{\partial x_i}\left(\bar{\rho}\frac{\nu+\nu_t}{Sc_l}\frac{\partial \tilde{Y}_l}{\partial x_i}\right) + \dot{\tilde{\omega}}_l + S_l \tag{4.21}$$

The transported quantities k and ϵ are transported accordingly

$$\bar{\rho}\frac{Dk}{Dt} = \frac{\partial}{\partial x_i}\left(\bar{\rho}\left(\nu + \frac{\nu_t}{\sigma_k}\right)\frac{\partial k}{\partial x_i}\right) + P_k - P_\epsilon \tag{4.22}$$

$$\bar{\rho}\frac{D\epsilon}{Dt} = \frac{\partial}{\partial x_i}\left(\bar{\rho}\left(\nu + \frac{\nu_t}{\sigma_\epsilon}\right)\frac{\partial \epsilon}{\partial x_i}\right) + P_\epsilon - D_\epsilon \tag{4.23}$$

This completes the RAS formulation.

4.3 Multiphase modeling

The injection and breakup of liquid fuel in a combustion engine is composed of a liquid phase which needs separate treatment. Multiple methods exist for detailed surface tracking in gas/liquid interaction but due to the extreme levels of turbulence in ICEs such methods are rarely used as the required resolution to treat small cusps in in the surface is very high. More often in engine simulations statistical methods of liquid droplet representation are used. One such concept of methods can be grouped into the Lagrangian particle tracking class.

4.3.1 Lagrangian particle tracking

The fuel injection in all papers containing a spray is modelled using Lagrangian particle tracking (LPT) method which represents the statistical distribution of fuel droplets by tracking groups of droplets with identical properties (the so-called parcels) which interact with the gas flow in a 2-way coupling. The interaction is described by the following equations of motion.

$$\frac{d}{dt}\vec{x}_p = \vec{u}_p \tag{4.24}$$

$$\frac{d}{dt}\vec{u}_p = \frac{C_D}{\tau_p}\frac{Re_p}{24}\left(\vec{u}_g - \vec{u}_p\right) = \frac{C_D}{\tau_p}\frac{Re_p}{24}\vec{u}_{rel} \tag{4.25}$$

Here the parcel Reynolds number is defined as $Re_p = |\vec{u}_{rel}|d_p/\nu$ and the relative velocity between gas and parcels $\vec{u}_{rel} = \vec{u}_g - \vec{u}_p$. The drag coefficient C_D is given as

$$C_D = \frac{24}{Re_p}\left(1 + \frac{1}{6}Re_p^{2/3}\right), \qquad Re_p \leq 1000 \tag{4.26}$$

$$\text{or } 0.426, \qquad Re_p > 1000 \tag{4.27}$$

In order to include the effects of the unresolved flow on the relative velocity $\vec{u}_{rel}$ we estimate the velocity according to the O'Rourke model [76], where relative velocity is decomposed as:

$$\vec{u}_{rel} = \tilde{\vec{u}} + \vec{u'}_p - \vec{u}_p \tag{4.28}$$

where $\vec{u'}_p$ is stochastically taken from a Gaussian distribution with a standard deviation $\sigma = \sqrt{2k_{sgs}/3}$ for each parcel's progression (insert k for RAS). The momentum transport equation source term is calculated from a single cell as

$$\bar{S}_{u,i} = \frac{1}{V_{cell}} \sum_{p} \left(m_p \frac{d}{dt} u_{p,i} \right) \tag{4.29}$$

where the sum goes over parcels in the cell and source terms for the continuity, enthalpy, and species equations are modelled similarly. For each cell and time step the source terms of all parcels are summed up into the final source term in the corresponding equation.

The injected size distribution of the parcels is pre-specified and chosen randomly from a Weibull distribution with a k-parameter value of 3 and an average diameter of 30 μm. The secondary breakup of the droplets is modeled using the Kelvin-Helmholtz/Rayleigh-Taylor model with standard coefficients as seen in [77] and a break-up timescale coefficient B_1 of 40. Wall/parcel interaction is handled by a partially plastic rebound on wall collisions. The Ranz-Marshall correlation is used to compute the heat exchange between the droplet and the gas while the evaporation is modelled by the Frössling equation. The injection profile of the spray is set to a top-hat profile and the discharge coefficient is set to 0.7.

4.4 Transported chemical kinetics

The chemical reactions are described in a transported chemical kinetics scheme. These schemes give information on coefficients in the equations shown in section 3.2. There are multiple types of mechanisms for each fuel type, and usually the full mechanisms contain hundreds if not thousands of species and even more reactions. Solving ODE for so many species cannot be done in full 3D so it's common to find reduced or skeletal versions of the full mechanisms in reacting CFD. These skeletal mechanisms focus on capturing ignition delay times in a small and specified range of operations. Often certain types of chemical branches are required as well, like the ketohydro-decomposition of n-heptane which is responsible for cool flames. For the reacting flow simulations presented in this thesis the Liu skeletal mechanism was used [78], which is specialized in LTC combustion of PRF fuel containing varying ratios of n-heptane and iso-octane. The Zel'Dovich NO_x mechanism was implemented to model such emissions.

4.4.1 Chemistry speedup algortithms

Once calculated, the chemical reaction rates are integrated into the transport equations using chemistry coordinate mapping, a speed-up algorithm [79], in which calculations of the reaction rates are not performed for individual mesh cells but rather for groups of cells. The grouping is based on a chemistry phase space which is made up of four dimensions in the works presented in this thesis: a progress variable based on element mass fractions, scalar dissipation rate, temperature, and mass fraction of nitrogen gas. In general the average speed-up during the main combustion event is around a factor of six. For paper II the fuels are included as well.

4.5 Interaction between chemistry and unresolved turbulence

Unless specified otherwise, in a filtered simulation the chemistry is dependent only of mean values, which might not always be true. Because of this separate models for treatment of the effects of the unresolved fields on the chemistry are needed. Three different methods are used in the works of the thesis; direct integration, and the partially stirred reactor.

4.5.1 Direct integration

The direct integration of reaction rates means that the reaction rate output from the chemical equations in section 3.2 are simply integrated in time to calculate the total chemical change rate in equation 3.4. No input from the unresolved fields is used which implicitly means that the mixture is assumed to be very well mixed and forces from the unresolved momentum are small. For this reason the model is also called the well stirred reactor (WSR).

4.5.2 Partially stirred reactor model

Conceptually developed for non-premixed combustion this model assumes that in each cell some part of the cell is in an unmixed state. This state correlates with the ratio of chemical to turbulent time-scale seen in equation 4.31. The reaction rate is then scaled in accordance to the level of unmixed reactants as seen in equation 4.30.

$$\dot{\tilde{\omega}}^{PaSR} = \kappa \cdot \dot{\tilde{\omega}} \tag{4.30}$$

$$\kappa = \frac{\tau_c}{\tau_c + C_{mix} \cdot \tau_t} \tag{4.31}$$

The simple analogy can be interpreted in terms of the unresolved stratification as well. If used to model an ignition front, the implicit assumption is that the slow down due to unresolved stratification is proportional the function of time-scales seen in equation 4.31, in other words; large scale turbulence means high stratification.

4.5.3 Eulerian stochastic fields

A more detailed statistical treatment of the unresolved fields can be achieved by using a transport equation for the probability density function of some selected fields. Because turbulent reacting flows are highly dependent on the small scale fluctuations of chemical species the PDF modelling is usually applied to the chemical components. There are several methods to achieve this, but in the work presented in this thesis the Eulerian stochastic fields method is used.

The stochastic fields method progresses multiple separate instances of the simulation, that individually lack a physical meaning, here called stochastic instance simulations. Each

transported quantity that will be modelled using a transported PDF (like for example temperature) has a separate representation in each stochastic instance simulation. For every such quantity, in every stochastic instance simulation, in every cell, a perturbation is added - the so called Wiener term (WT).

$$WT = \bar{\rho}\sqrt{2\frac{D_t}{\bar{\rho}}}\frac{\partial\phi}{\partial x_i}dW \tag{4.32}$$

here D_t is the effective total diffusivity (or conductivity), ϕ is the stochastic instance field and dW is a stochastic random vector chosen from a normal distribution. This represents the "random" transport from unresolved scales. In order to model the diffusive effects from turbulence, the so called mixing term, MM, is implemented by interaction with the mean of all the stochastic instances:

$$MM = -\frac{\bar{\rho}}{2\tau_k}\left(\phi - \bar{\phi}\right) \tag{4.33}$$

where $\bar{\phi}$ is the mean value for ϕ of all stochastic instances. Both these terms are applied to the transport equation of the transported quantity in question to model the progression of the stochastic instances. The proper physical quantity is then the mean value $\bar{\phi}$ and higher order moments of it's PDF can be calculated from the stochastic instances.

Chapter 5

Summary of results

This chapter presents the findings of the research, summarized into three sections. First, the general characteristics of flow in PPC engines are discussed in combination with the simplifications common in CFD modelling of engine combustion. The second part discusses how the ignition kernel is formed and how the initial distribution of physical properties characterizes the ignition event. The third part discusses the findings of how a reaction front in a PPC engine can be tracked, studied and modelled in a CFD framework.

5.1 Flow in PPC engines

At the beginning of the research project, publications containing CFD simulations of combustion in PPC-like environments had been available for nearly a decade. The methodology for describing such combustion was not as well established as in CDC simulations. Diesel engine simulations performed in periodic sector domains using RAS can give robust results because the physical characteristics which describe the process are periodically occurring and the scales responsible for the flame/turbulence interaction are very small and described well by the Boussinesq approximation. SI engine simulations on the other hand, are almost exclusively performed in a full cylinder simulation, where more focus is put on proper turbulence modelling.

PPC engines often include multiple combustion modes, stratified premixed charges and an ignition process which is strongly dependent on the level of mixing and has a vary wide range of outcomes. Because of this, more information on which flow characteristics are critical to properly model a PPC combustion event was studied in papers I and III. In order to understand which simplifications can be allowed in the PPC engine, an investigation into the turbulent mixing occurring at typical PPC injection timings was started.

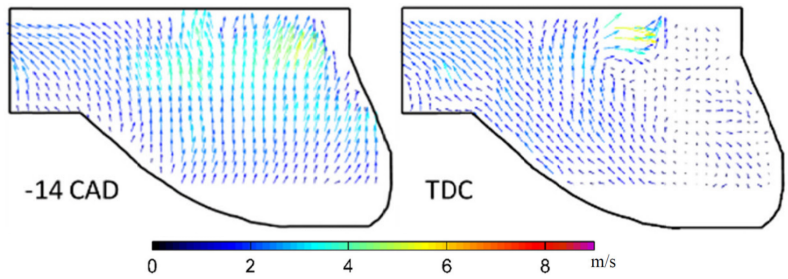

Figure 5.1: Experimental PIV results showing the cycle average planar velocity field of the motored case of a Volvo I5D optical research engine with a Diesel-like piston bowl at 14 crank angles and 0 crank angles before the TDC. The plane is reportedly cut through the center of the cylinder. The upper left corner of the field shows a flow through the center of the cylinder. Borrowed with permission from author [80].

5.1.1 Swirl structure progression

A cycle average flow study presented by Wang et al. [80] includes planar PIV measurements through the center of the in-cylinder flow. Some results from said paper, seen in figure 5.1, show a cycle average planar flow component through the center of the cylinder, meaning that the swirl is not rotating around the center with a tangential symmetry. PPC engine simulations are often performed in periodic cylinder domains and an asymmetric swirl would give such an approach less validity.

To investigate the cause and influence of such a flow in PPC engines a numerical study of a semi-open cycle was performed in the same geometry by utilizing the mesh deformation technique described in section 4.1.3. The results of this study show that the tilt of the swirl motion is changing constantly from the moment of swirl structure formation. Since the tilted swirl motion rotates around its own axis, some measurement method which is independent on the local orientation of the swirl structure is needed for quantification. In analogy to how swirl is calculated by the axial projection of the angular momentum vector (see equation 3.18), a projection of the angular momentum vector onto a plane perpendicular to the cylinder axis was used as seen in figure 5.2.

$$L_{xy} = \int_m r \times u \cdot dm \cdot \frac{\hat{x} + \hat{y}}{\sqrt{2}} \tag{5.1}$$

where r is the vector distance from the center of mass, u is the velocity vector, $\hat{x}$ and $\hat{y}$ are unity vectors in x and y direction (z being the direction of the piston axis).

The angular momentum vector progression on the plane perpendicular to the piston axis shows how the total level of asymmetry varies with time and that the most asymmetric behaviour occurs before IVC. After the closing of the valve, the swirl center seems to be slowly stabilized by the shape of the piston bowl. Since the angular momentum vector is

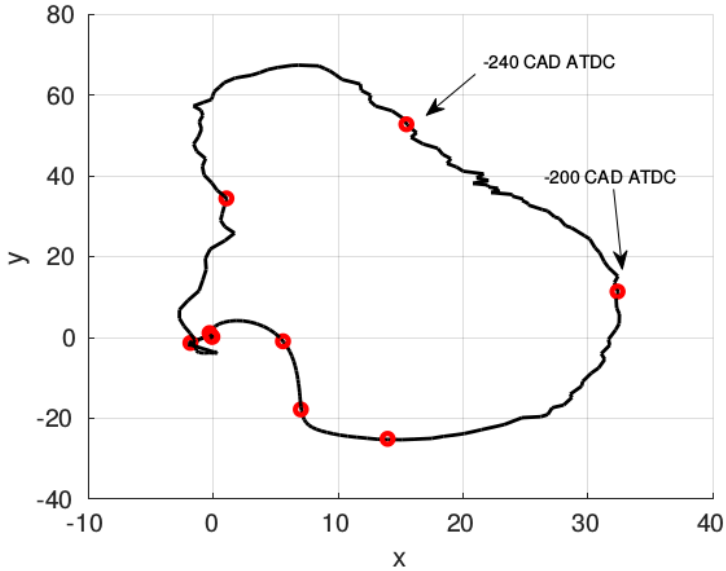

Figure 5.2: The progression of the angular momentum vector projected over a plane perpendicular to the piston axis. The asymmetry shows a clockwise progression with the red dots denoting time intervals of 40 crank angles. IVC occurs at -160 CA aTDC.

an average quantity of the total in-cylinder flow, it can not give any more information on how the asymmetric components are distributed. A more local measure is introduced to study how the swirl structure varies with the piston axis. By dividing the flow along the piston axis into multiple planar flow structures and identifying the center of rotation in those 2D-slices a distribution of swirl centres along the axis can be observed, see figure 5.3. The asymmetric behaviour seems to stop at -20 CA aTDC in the simulations which does not match the PIV flow measurement seen in figure 5.1.

There are some possible explanations for this; either the RAS could not capture the average rotating structures which are observed or the experimental plane did not properly cross the cylinder center. In the latter case, the asymmetric flow at the center of the cylinder could actually be a part of the swirl. It is also possible that the ensemble-average observations of the experiments are not representative of the true cycle average. In any case, flow structures similar to the experiments were observed prior to -20 CA aTDC as seen in figure 5.4, where it is also shown that a periodic sector simulation mapped from the full cylinder can not recreate the effect.

The mixing effects from a non-axially symmetric swirling structure are treated in section 5.1.3.

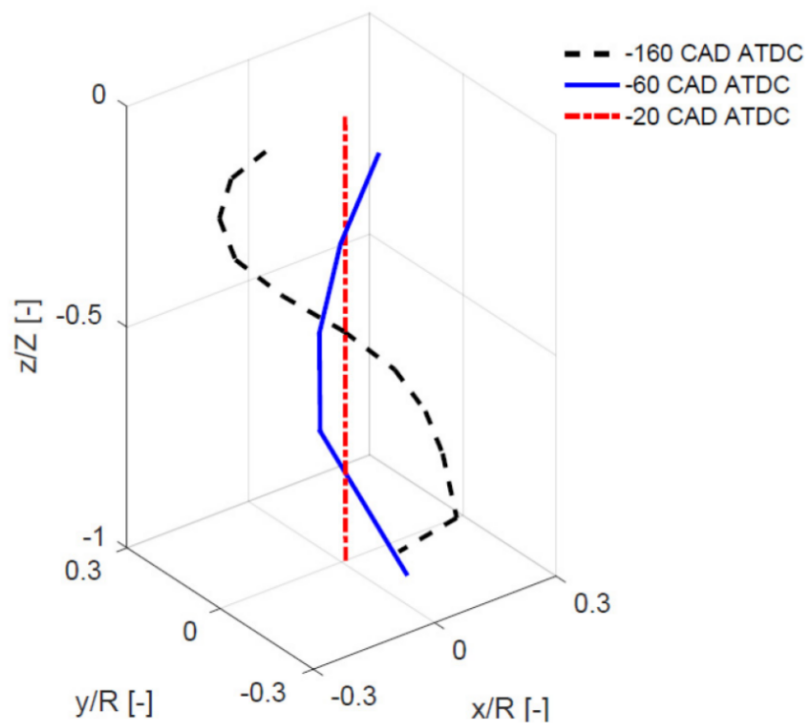

Figure 5.3: The calculated swirl center progression in time. The units are normalized by the span of the computational domain.

5.1.2 The periodicity assumption

The next investigation in the flow analysis project covers the validity of the periodic sector assumption as well as an investigation into the relevance of the swirling initial conditions in the LES formulation. Section 5.1.2 discusses the periodic sector and section 5.1.3 treats the initial conditions.

In this section, the effect of periodic sectors on turbulent mixing and the state of fuel and temperature distribution prior to ignition is studied in a set of non-reacting PPC engine cases. The idea is to compare mixing of the same turbulent field taken from a full cylinder simulation and map it to a periodic sector. The study is focused on combustion simulations and so a sector simulation field is mapped from the full cylinder simulation at the moment of injection and the progression of the two simulations are compared. A near-identical mesh is used in both cases to make the comparison independent of the numerical filtering, except for the periodic transform. Three different injection timings, representing a range from PPC to late HCCI, are investigated. These timings are selected to represent characteristic cases of all fuel injected into the piston bowl (SOI-17), fuel split between bowl and

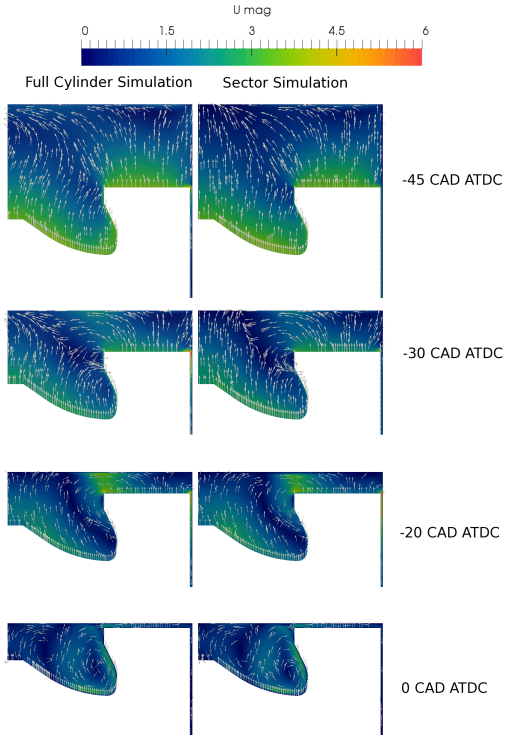

Figure 5.4: A comparison of the time progression of the planar velocity field between the full cylinder case and the sector case. As can be seen the full cylinder field has a flow component moving through the cylinder center.

squish (SOI-29) and all fuel in the squish (SOI-54).

A realistic initial condition is created by mapping the Reynolds average flow from the open cycle simulation discussed in section 5.1.1 to a constant volume domain at the time of IVC. The small scale turbulence then develops over time, and after a certain time, the root-mean-square of the velocity field converges on a certain value. The velocity and pressure fields are then mapped as initial condition for the full cylinder simulation. As the full cylinder simulation reaches the SOI, the sector simulation is then mapped from the full cylinder field, see figure 5.5. The initial turbulent momentum field distribution can be seen in figure 5.6.

The analysis of temperature and mixture fraction distributions can be summarized in the following observations:

- During the injection, the variance in terms of temperature and mixture fraction distribution between sprays is very small in the full cylinder simulation for all cases. The sector simulation has nearly identical distribution functions as well.

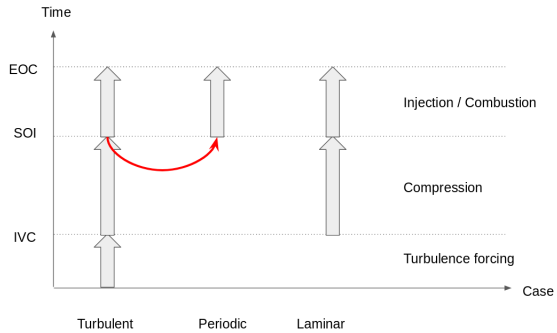

Figure 5.5: Schematic picture of how initial conditions are generated for the different cases. The red arrow shows the mapping from the turbulent case to the periodic. Times denoted are intake valve closing, start of injection and end of combustion

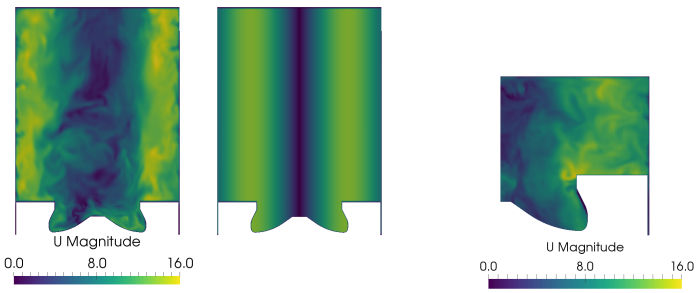

Figure 5.6: Initial velocity distribution in a turbulent case, laminar case and mapped sector case. The sector case is mapped at a later time than the full cylinder cases.

- After injection, at intermediate stages of mixing, the distributions retain a very similar shape for the -17 and -29 injection timings, but not for the earliest timing.
- Around TDC, all three injection timings show noticeable errors in distribution, but the strongest difference is visible in the -17 injection timing, and the smallest difference for the -29 injection timing.

Figure 5.7 shows the fuel rich and hot gas mixtures at TDC in the full cylinder and sector simulation. In this image, the difference in mixing at the central part of the cylinder becomes visible. In the full cylinder simulation, the distribution of fuel rich mixture fraction covers a much larger volume. The PDF distribution of mixture fraction in full cylinder and sector simulations shows a similar difference, as can be observed in figure 5.9. Some mixture fraction and temperature values are ”frozen” in the sector simulations and do not mix with the ambient gas at the same pace. Spatial analysis of these pockets of gas shows that they are exclusively located close to the cylinder center in the sector domain. The same analysis is performed for the other injection cases which leads to a conclusion: Due to unrealistic dissipation of flow structures outside the domain, which are not symmetric

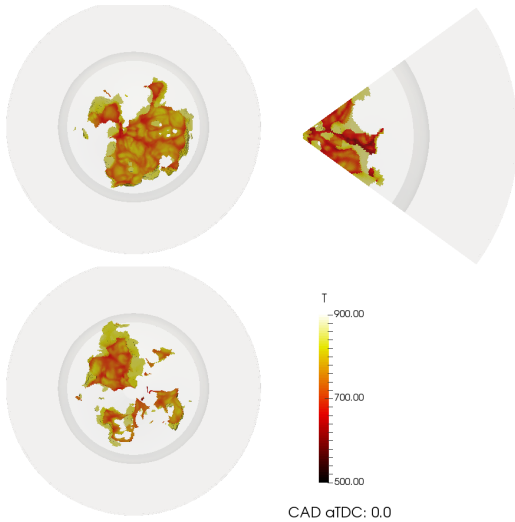

Figure 5.7: Comparison of mixture fractions above 0.046 in at TDC for a single injection starting at -17 CA aTDC. The surfaces are coloured by temperature. The top left image shows the turbulent full cylinder simulation and the top right image the sector simulation. The bottom image shows the full cylinder simulation using laminar initial condition.

around the cylinder center, the sector mesh does not represent mixing close to the cylinder center in a proper way in LES turbulence formulation. This conclusion can explain why the late injection case showed the biggest error in the sector simulation - the re-entrant piston bowl shape means that the fuel is redirected towards the cylinder center. The full data of resulting distributions of mixture fraction and temperature can be seen in paper III, as well as other observations.

5.1.3 Initial conditions

In RAS it is common to initialize a swirling flow field at IVC with a simple radial velocity component which has a magnitude based on its radial coordinate according to a Bessel function of the first kind. Because RAS means that the turbulent flow is presented as a cycle average quantity, the initial conditions of the turbulent field have a tendency to quickly converge towards a certain value, as long as the initial conditions are not chosen too poorly. For this reason, it is not uncommon to set the turbulent kinetic energy and turbulent dissipation fields to uniformly distributed values with some educated guess for magnitude.

For the LES turbulence formulation, the importance of initial conditions is more important. Since the filtering only occurs at a scale size basis the choice of initial conditions affects the progression of the simulation very much, and a small difference in initial conditions often yields a much different outcome. Most publications using LES in swirling engine geometries tend to have a very simple initial flow field estimate akin to the methods

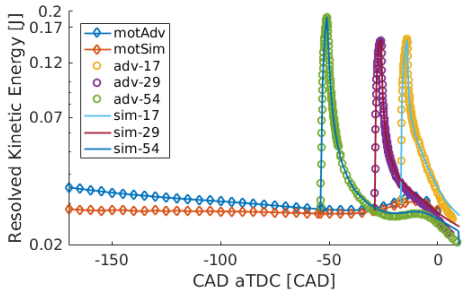

Figure 5.8: Resolved total flow kinetic energy for the full cylinder cases.

presented for RAS.

A comparison of the distribution of mixture fraction and temperature in the gas prior to ignition is used to investigate the validity of the sector assumption in section 5.1.2. An identical analysis is now performed on two very different initial conditions, in order to get an estimate of what effect such a choice can have in LES simulations. This time no sector assumption is applied, and two full cylinder simulations are compared. The same initial condition as described in section 5.1.2 is used, but is now compared to a laminar flow initial condition. The turbulent initial condition is referred to as the advanced case and the laminar as the simple case. A comparison of initial flow structures can be seen in figure 5.6. The same three injection timings are investigated, -17, -29 and -54 CA aTDC.

The temperature and mixture fraction distributions are very similar during, and just after, the injection in both the advanced and simple cases for all injection timings. This is expected as the kinetic energy introduced by the spray is several times higher than that of the flow. Nevertheless large differences in the mixing occur at around 10 crank angles after injection and continue to grow with simulation time. The resulting differences for temperature and mixture fraction distribution in the -17 CA aTDC injection case can be seen in figures 5.7 and 5.9.

The swirl structure of the advanced flow has a much faster decay rate since the flow component, which is not cylindrically symmetric, encounters a higher flow resistance due to geometry. This is reflected in the PDFs of mixture fraction since the simple case has an offset towards the fuel rich side compared to the advanced case. In general, the simple case

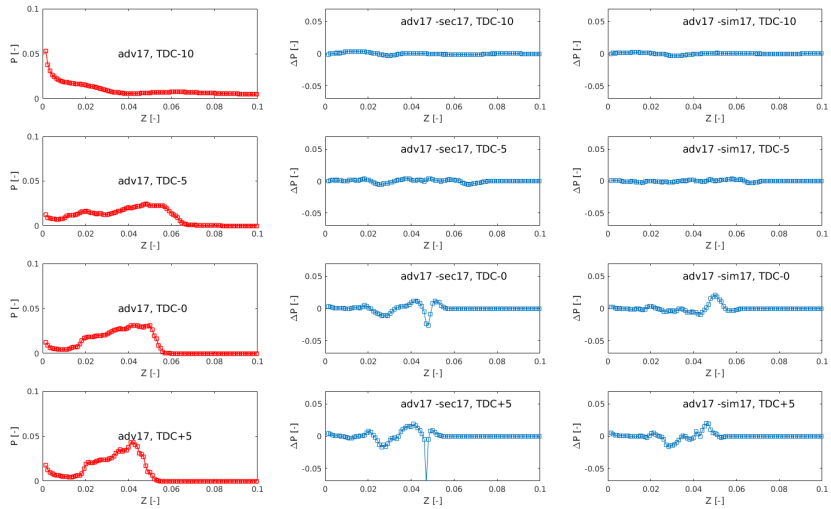

Figure 5.9: PDFs of the mixture fraction distribution at times close TDC after injecting at -17 CA aTDC. The left column shows the full cylinder simulation with turbulent initial condition, the middle column shows the sector simulation mapped from the advanced simulation, the right column shows the laminar initial condition, but with the same swirl as the turbulent condition.

has a higher level of swirl while the advanced case has a higher level of turbulence and hence turbulent mixing.

5.2 RAS approach to PPC combustion modeling

The second part of the result section treats the modelling of combustion processes in direct injected engines running in PPC or HCCI mode. A sweep of injection timings in a DICI engine is analysed - the combustion phasing (CA50) is kept constant and intake conditions are varied to achieve this. The study is performed with RAS and no additional model compensating for unresolved scalar stratification or effects from unresolved momentum on combustion. Due to the difficulties described in section 2.3.4 the exact fuel mass is an estimate based on pressure trace and model estimations.

A very important characteristic for this study is the extremely low load of the case. This affects the type of combustion occurring in the engine since the mixture of fuel and oxidizer will always be leaner than stoichiometry and no non-premixed combustion can occur.

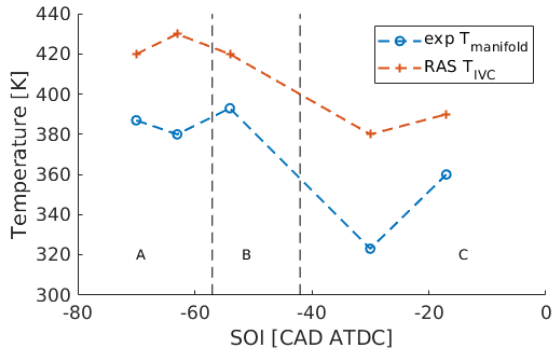

Figure 5.10: Comparison between experimental and simulated required intake temperature values to reach constant CA50 for different injection strategies.

5.2.1 Required intake temperature

In a RAS model, the transported fields represent the spatial distribution of the cycle average value of the scalar in question. All subsequent interaction between transported values, like chemistry, will be a function of mean interaction. However, the real ignition process is not an interaction of mean values, because ignition does not occur at the average temperature but rather the hottest (and in fuel analogue, the richest). In RAS these ”hottest” and ”richest” locations are not known and while it is possible to say where the hottest average temperature will be, small hot and rich pockets occur due to turbulent fluctuations. Such fluctuations are quantities which are not represented in the Reynolds-average flow.

The required intake temperature for combustion to occur in a RAS is therefore always higher than the experimental value unless turbulent stratification of scalars is somehow implemented. The required intake temperatures in figure 5.10 used the well stirred reactor assumption, and are therefore consistently higher than the experiments. Despite all this the trend is reproduced in all cases except for the SOI -63 CA aTDC case - a case which ignited very close to a wall.

A side comment on intake temperature can be given; besides the turbulent fluctuations there are other effects which disturb the required intake temperature of a simulation. Heat losses during the compression cycle depend on guessed temperatures at the walls (usually constant temperatures with no coupling to gas temperature) as well as wall modelling to estimate effects of wall turbulence on heat transfer. Additionally the chemical mechanism might not perfectly represent the ignition delay time, causing the gas to ignite at wrong time.

5.2.2 Comment on compression ignition

The ignition process is described by the ignition delay time τ_i. This time is simply defined as a count-down clock to some defined moment of the ignition of a particular gas mixture with a particular thermodynamic state at constant volume. In a combustion engine undergoing compression, the ignition delay time will be continuously shortened by changes in the thermodynamic state (due to compression), as well as the natural progression of the chemical kinetics. A simple example model is presented to illustrate the effect.

In a simplified case where the ignition delay time only depends temperature, a differential expression of the progression of the true "compressing" ignition delay time τ_i^* would be:

$$\frac{d\tau_i^*}{dt} = -1 + \frac{d\tau_i}{dT}\frac{dT}{dt} \tag{5.2}$$

where T is the gas temperature variable, t is time and the -1 term defines the unperturbed chemical progression. Using a simple model of temperature progression:

$$\frac{d\tau_i^*}{dt} = -1 + \frac{d\tau_i}{dT}\frac{d}{dt}\left(T_0 \cdot r_{c0}(t)^{\gamma_{eff}-1}\right) \tag{5.3}$$

where $r_{c0}(t)$ is the time dependent compression ratio in reference to some initial condition and T_0 is the temperature at such a condition. Entropic losses are accounted for by an adjusted ratio of specific heats, γ_{eff}. By comparing the first and second terms on the right hand side of equation 5.3, we can see if the compression of the gas is changing the ignition delay time faster than the natural progression of the chemical kinetics.

An analysis is made by simple estimations of the temperature derivative of τ_i obtained using the Liu kinetic scheme in constant volume reactors. While the gas is relatively cold during early stages of compression, the natural ignition delay time is so long that the compressive effect dominates. Since the first ignition kernel occurs around TDC, where the cylinder temperature is rather constant prior to ignition, the left term is dominating. Explained in the often used equivalence ratio / temperature space, $\phi - T$, the compression pushes the fuel high enough on the temperature scale for natural ignition delay time to take over, cf. figure 5.12. If the compression pushes the fuel too far on the temperature scale, a premature ignition event occurs which is driven by the piston movement. This effect is called engine knock and is particularly dangerous as the term on the right is very large during the compression and can cause ignition front displacement speeds that reach Mach 1, which can couple momentum, thermodynamics and chemistry to form detonation fronts [81].

Once the fuel mixture reaches this characteristic value of ignition delay time, the combustion starts. As soon as a heat release occurs, the right term becomes dominating and equation 5.3 is no longer valid as the chemical heat release dominates the temperature

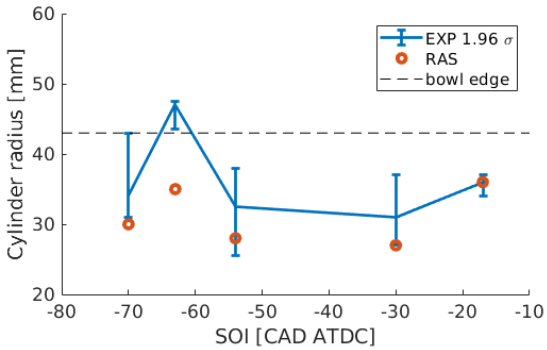

Figure 5.11: Comparison between experimental cycle average radial ignition location distribution to RAS simulation for different injection strategies.

change of the ambient gas due to the thermal expansion of the reacting gas. This is often referred to as the ”limited volume effect” of combustion engines and means that the progression of auto-ignition is actually a chain effect of ignition of other fuel matter. These effects together form the ignition front ”propagation”.

5.2.3 Ignition location

A comparison of radial ignition coordinates between simulations and natural luminosity from optical experiments are seen in figure 5.11. While the correct trend can be seen in most cases, the difference grows with incumbent mixing time. The early injection timings are harder to predict.

One explanation for this could be that early injections have turbulent stratification of scalars which is largely independent on resolved quantities, while the late injections should have stratification which is tightly coupled to the mean flow (gradient proportional to variance). Furthermore a large part of the main combustion in the early injection is seen to occur near the center of the cylinder in the experiments. Sprays in RAS are known to be too diffusive due to the Boussinesq assumption - this might also cause further transport of fuel to be diffused into a uniformly distributed cloud at an early stage.

5.2.4 Ignition prediction

By analysing the state of fuel and equivalence ratio of the ignition kernel in each case a result such as in figure 5.12 can be observed. The location of the ignition kernels follow the

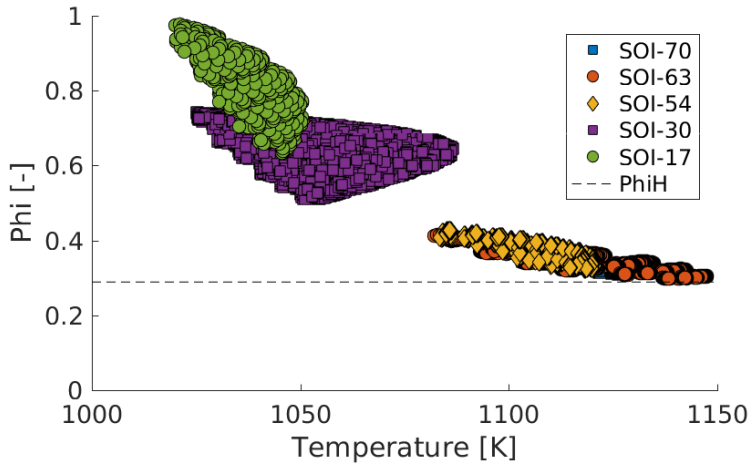

Figure 5.12: Equivalence ratio and temperature cell value of the ignition kernels from each injection strategy in a ϕ-T scatter plot. The dashed line shows the homogeneous mixture equivalence ratio.

shape of an iso-line of ignition delay times in the $\phi - T$ space. This again shows that there exists some characteristic ignition delay time which occurs just prior to the ignition process.

If one plots the progression of the full gas mixture cloud in the $\phi - T$ space it soon becomes clear that as the cloud is compressed it moves to the right of the graph in a uniform motion until small part of the cloud reaches a characteristically small ignition delay time at which time ignition occurs. It is therefore possible to predict the location of an ignition kernel with reasonable accuracy simply by looking at how the fuel cloud advances towards ignition in the $\phi - T$ space.

Cool flame reactivity which occurs prior to the main ignition shifts the temperature of richer mixtures which in turn disturbs any ignition predictions. Depending on injection timing such a cool flame effect will vary in strength.

5.2.5 Reaction front propagation

Reaction front propagation is of utmost importance in engine configurations where the fuel is distributed over the cylinder volume. In PPC engines the heterogeneous distribution of fuel and temperature can cause varying types of reaction front behaviour. If the combustion happens too fast the pressure rise rate endangers the engine's structural integrity while too slow combustion causes incomplete fuel consumption.

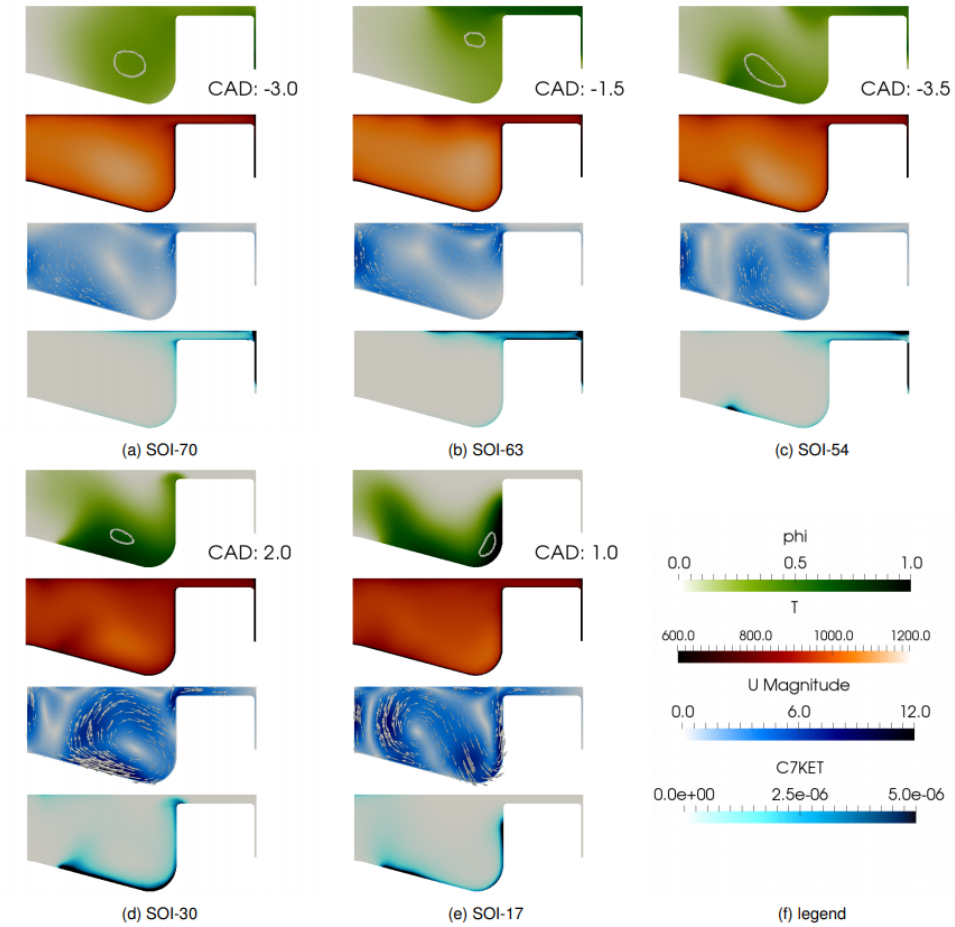

Figure 5.13: Cuts through the center of the cylinder at the (separate) moment of ignition for five injection cases. Equivalance ratio, temperature, velocity magnitude and ketohydroperoxide decomposition are visible for each case. The white circle inside the equivalence ratio distribution depicts the ignition location.

Figure 5.14 shows the pressure traces of the simulations in comparison to the cycle average pressure traces of the experiments. As pressure traces can be considered as validation data-sets for the average pace of heat release in the engine there are some noticeable differences in the data match of the injections. It is easy to observe that the later injections cause faster combustion while early injections cause slow combustion. Generally this trend is predicted in the simulations but the speed of late injection combustion in the simulation is too high.

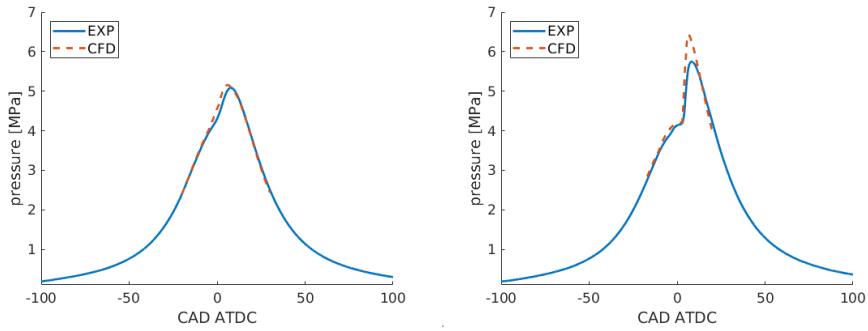

Figure 5.14: The cylinder average pressure trace of two injection timings for both simulations and experiments in a Scania D13 Optical engine. The left side shows the SOI-54 case and the right side shows the SOI-17 case. The early injection cases show relatively good agreement, while the late injections show too violent combustion.

Initially both experimental and simulated results seemed a bit counter-intuitive to the author since late injections have much higher stratification in temperature and fuel concentration, c.f. figure 5.13. HCCI is generally believed to result in much faster combustion due to the homogeneity of fuel concentration. A linearised estimation of the gradient $\nabla\tau_i$ with respect to T and Z becomes

$$\frac{\partial \tau_i}{\partial x} = \frac{\partial \tau_i}{\partial T} \cdot \frac{\partial T}{\partial x} + \frac{\partial \tau_i}{\partial Z} \cdot \frac{\partial Z}{\partial x} \tag{5.4}$$

Experiments show reaction front speeds in the range of 100 m/s which imply that an ignition front is at least partially responsible for the reaction front propagation which again makes no sense with large stratification of τ_i. To explain the phenomenon a hypothesis is put forth that in fact the stratification in ignition delay time is larger for the homogeneous cases than the late PPC injections. The reasoning behind the hypothesis is that while the stratification of transported scalars was higher for the late cases the kinetic dependence on temperature and fuel concentration are even more important:

$$\left|\frac{\partial \tau}{\partial T}\right|_{lean} > \left|\frac{\partial \tau}{\partial T}\right|_{rich} \tag{5.5}$$

$$\left|\frac{\partial \tau}{\partial Z}\right|_{lean} > \left|\frac{\partial \tau}{\partial Z}\right|_{rich} \tag{5.6}$$

for example, a near-homogeneous distribution of a very lean fuel charge will encounter a very large inhomogeneity in ignition delay times despite only having a very small stratification in fuel concentration. Such a hypothesis could explain why combustion in the late injections of the RAS are much faster than the experiments, since very large stratification in Z and T would be needed to cause a measurable stratification in τ_i. If the hypothesis holds true the unresolved stratification of Z and T in the RAS is key to capturing the progression

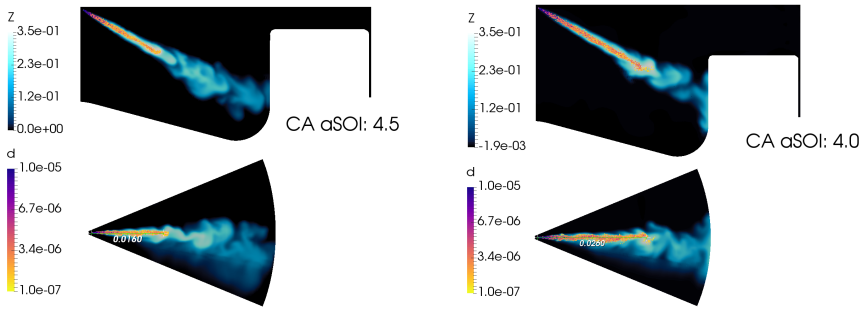

Figure 5.15: Simulated spray image of the LES of the Scania D13 optical engine. The image shows mixture fraction in cross sections trough the center of the spray for injection timing -17 CA aTDC on the left and -30 CA aTDC on the right. Parcel average diameters are shown and the liquid length is matching the experimental value.

of the ignition front. For this reason the late injections of the current case are simulated using the large eddy turbulence formulation in the next section.

5.3 LES approach to PPC combustion modelling

In order to include some information on temperature and chemical component stratification by turbulence an LES turbulence model is used in the following work. The same engine conditions as described in section 5.2 are now simulated using LES but only for the two latest injections. Injection timings -17 and -30 CA aTDC are repeated using a closed cycle setup. Again because experiments show that the reaction fronts propagate at around 100 m/s, the ignition front combustion mode is assumed to be the driving mechanism behind the reaction front displacement. Because of this the small scale turbulence effects on combustion are omitted and a direct numerical integration (well stirred reactor combustion model) of reaction rates is applied.

In order to acquire proper initial flow conditions a turbulence forcing technique is applied in a constant volume geometry - taken at the IVC state of the cylinder. In this full cylinder isenthalpic pre-simulation an initial condition of laminar flow is simulated so that a statistically stable energy cascade develops. To maintain the energy cascade kinetic energy is added to the largest scale (the laminar initial condition) so that the swirl number S_n is constant. This addition is performed once every 10 time steps in order to maintain the cascade. As the root mean square of the velocity fluctuations stabilizes around some mean value the energy cascade is considered to be stable and is transferred to a full cylinder compressing engine geometry at the moment of IVC.

The full cylinder is simulated throughout the compression stroke with full thermodynamic treatment. Small temperature inhomogeneities due to wall heat flux are enhanced in the

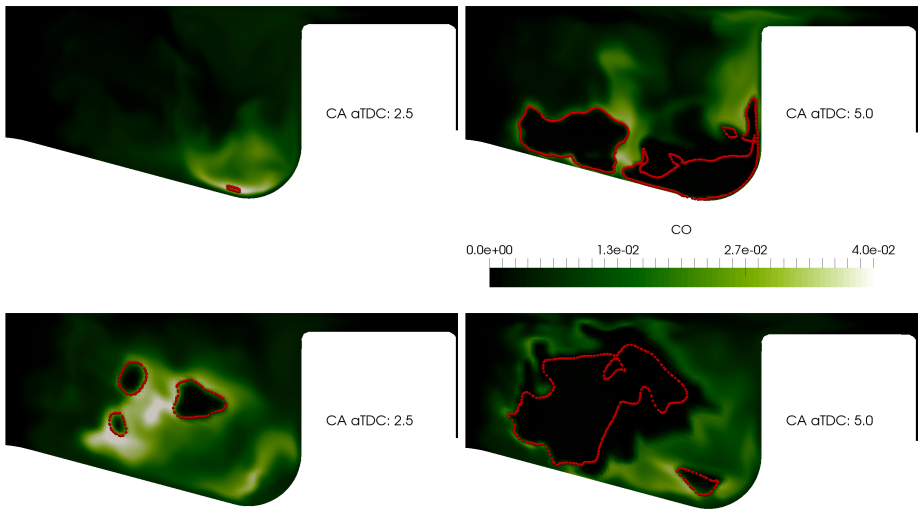

Figure 5.16: Top row shows progression of reaction front in case SOI -17 CA aTDC and bottom row in case SOI -17 CA aTDC. All images are taken from an LES in the Scania D13 engine. The green color shows mass fraction of CO. Planar reactivity speed is close to 100 m/s for the SOI -17 case which correlates well with the experimental values.

compression and mixed into the bulk flow, creating a stratified temperature field with local variations in the size of around 100 K. Due to the stabilizing effect of the geometry in the simulations the swirling motion is largely oriented along the piston axis. At SOI a cut of the flow field is mapped to a periodic sector.

Spray impingement images of the injection process can be seen in figure 5.15. The fuel vapour distribution is less diffusive than in the RAS and retains more of its momentum after impinging on the piston. Because the fuel distribution is different between the RAS and LES turbulence models it is hard to make direct comparisons of the combustion in each.

5.3.1 Ignition front

The resulting ignition front is decided by the distribution of CO and temperature fields. Once a sufficiently high cylinder temperature is reached the OH formation rate spikes and a high temperature reaction front is formed. Radial ignition location of the LES simulations occur within the standard deviation of experimental values in both cases. The reaction front propagation occurs at a speed comparable to the experimental images as seen in figure 5.16. Even though the distribution of fuel is quite different to that of the RAS model the same trend of increased combustion speed with later injection is reached. Pressure trace

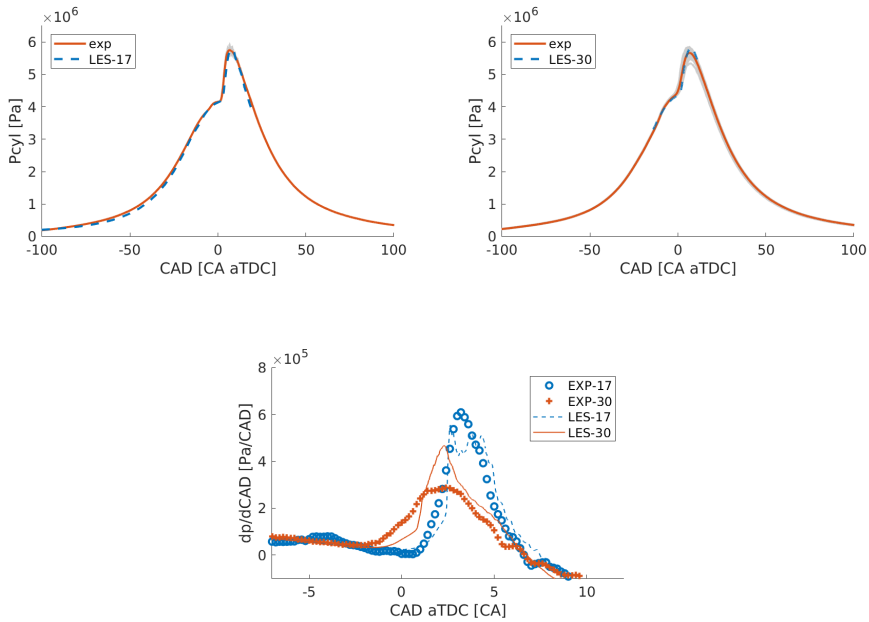

Figure 5.17: A comparison between LES and experimental results of cylinder average pressure and it's time derivative. A better agreement in terms of average pressure and pressure rise rate can be observed in the SOI -17 CA aTDC case, but both cases show much better pressure trace agreement than in the RAS model.

and pressure trace time derivatives are seen in figure 5.17. The good match with cylinder pressures despite using the same WSR model indicates that in fact the resolved fields of the LES simulation are required to properly model the ignition front.

5.3.2 Scalar stratification

The heterogeneous distribution of temperature and mixture fraction can be seen in figure 5.18. While the temperature distribution of both cases is relatively similar the later injection case tends to have higher fuel concentration. Based on these distributions in combination with the resulting speed of combustion it is possible to say that very large scalar variance is required to slow down combustion in late injection timings, while lower scalar variance is required for slowing down of earlier injections with a leaner fuel distribution. Thus it's possible to say that the large scale interaction with chemistry can sufficiently model the heat release and reaction front, which supports the hypothesis proposed in section 5.2.5. This does not exclude the use of the RAS turbulence formulation for PPC ignition fronts, but means that a separate treatment for unresolved stratification must be included for model fidelity.

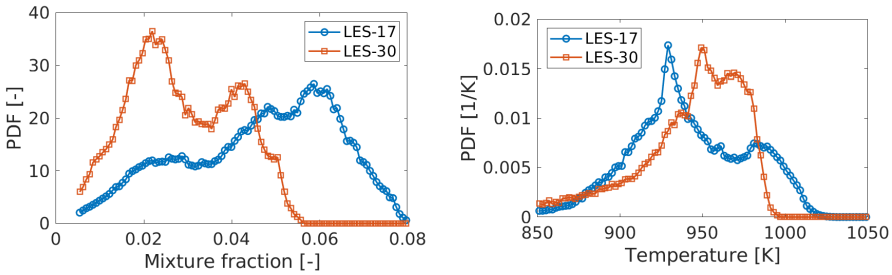

Figure 5.18: Distribution of mixture fraction and temperature at -5 CA aTDC (prior to reactivity) in LES cases of the Scania engine.

5.4 Mixed mode combustion in PPC engines

While large scale stratification is important to predict ignition front behaviour, deflagration is dependent on transport effects from the smallest scales. As previously mentioned it is not uncommon to find PPC engines operating in cases where mixed mode combustion occurs, and in fact all ignition fronts are by definition subsonic and as such are affected by momentum to some degree. This transition from auto-ignition to deflagration is not a well understood process, but is important because it determines the engines ability to burn overly lean fuel zones, which in the end affects combustion efficiency.

If a PPC engine has local mixture fraction values that are higher than the stoichiometric mixture fraction Z_{st} at the end of premixed combustion a mixing controlled combustion event will occur. This has some significant impact on the combustion process and subsequent engine characteristics. The combustion slows down considerably if the mixing controlled combustion is present, and what's worse is that it is dependent on the local state of the turbulence (near the stoichiometric surfaces of the fuel clouds). In CDC combustion such fuel clouds are always close to spray induced turbulence, but for PPC engines this is not necessarily the case.

To study how PPC engines behave under the conditions mentioned above and to validate which model set-ups are able to properly simulate such combustion a new numerical project is started. In this project the simulations are validated against the work presented by Wang and Lundgren [53, 82], where optical images showing planar distribution of fuel tracer, CH_2O formation and natural chemiluminescence of high temperature reactions in a late injection PPC case are studied in a very high temporal resolution (0.1 crank angles). With this data it is possible to validate the formation of premixed fuel ready to ignite, the premixed combustion planar propagation speed, and the location of the mixing controlled flame. The simulations are performed using the LES turbulence formulation to include

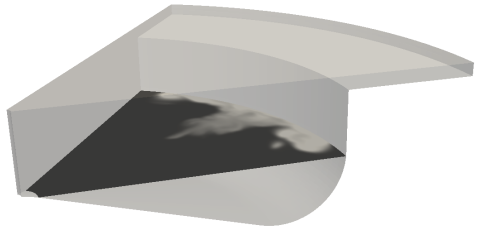

Figure 5.19: A picture of the experimental laser plane cutting through the Volvo D13 engine domain at TDC. The plane is located at a constant height and does not move with the piston.

realistic stratification and mixing effects. The experimental laser plane is located 12 mm below the cylinder head and has a normal aligned with the piston axis, cf figure 5.19. The fuel used in the experiment is PRF87 and the flow is quiescent.

5.4.1 PaSR approach

By applying the partially stirred reactor model to a combustion process containing ignition fronts some implicit assumptions are made. Specifically, in the modelling of a mixed mode reaction front propagating through a heterogeneous gas mixture the assumption that reactivity slow down due to unresolved stratification and transport from small scales is proportional to the time scale ratio in equation 4.31. This can be motivated by stating that low turbulence regions (high τ_t) are assumed to be more stratified than high turbulence regions, which in turn causes more slow-down due to unresolved stratification. Any potential speed-up effects occurring due to interaction between stratification and small scales are discarded.

Validation of CH_2O formation and distribution can be seen in figure 5.20 where matching distributions during and after the injection can be observed. This qualitative agreement implies that the pre-ignition reactivity and mixing effects are properly simulated which is important when modelling PPC engines since the distribution of τ_{i} (and thus the ignition front propagation) is entirely determined by this. The use of the specific spray model set-up and the Liu kinetic scheme [78] are thus well motivated in this case.

Despite only making out 13 % of the fuel volume the n-heptane has a strong impact on the ignition process. Almost immediately after SOI a ketohydroperoxide decomposition forms in the early shear mixing layer of the spray jet and releases its energy in a cool flame about the time it impinges on the piston bowl, cf. figure 5.22. Heat released from this cool flame

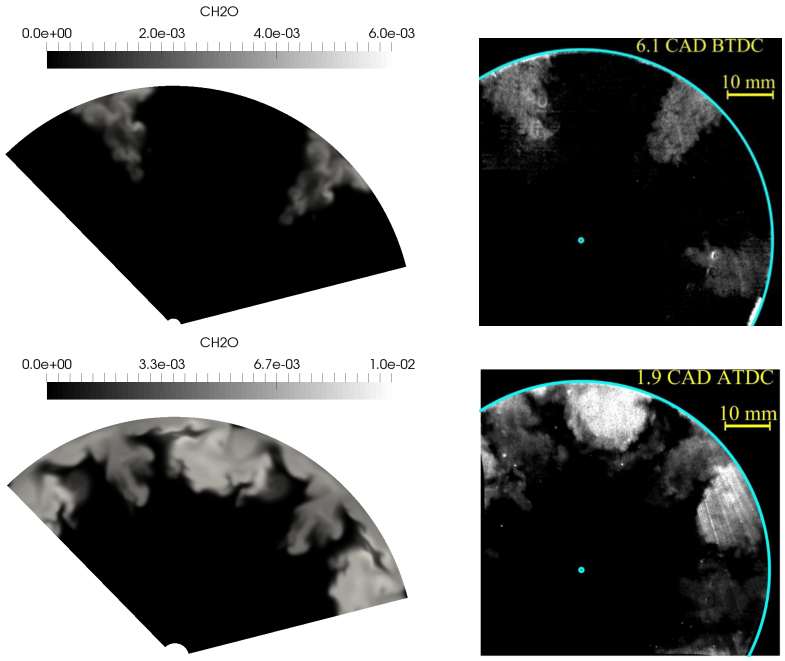

Figure 5.20: A qualitative comparison of CH_2O between simulations and experiments in a plane 12 mm under the cylinder head. The first row corresponds to -6.4 CAD aTDC and shows that CH_2O is formed during the spray. The second row corresponds to 1.8 CAD aTDC just prior to the ignition. The simulation domain is periodically duplicated to show the spray-spray interaction.

creates a small offset in temperature for parts of the fuel, and is a main factor for determining the ignition location. The heated fuel zone gets pushed out from the impingement location by the spray induced momentum. This outwards moving ring zone of slightly heated fuel gets distorted when it reaches walls or another spray plume. Tangentially the spray-spray interaction creates the classical recirculation zones seen in figure 5.20 and here the fuel remains in a rather cool state since two cold fuel clouds are mixing. In the other directions the outwards moving heated fuel ring encounters the piston bowl or cylinder head. Because the geometry forces the flow to redirect recirculation zones are formed where the slightly heated fuel is mixed with very hot oxidizer - this in turn causes two ignition kernels to form above and below the impingement location, close to the recirculation zones.

Due to the heat release in the ignition the reaction front expands rapidly (due to the mechanism seen in equation 5.2). Initial expansion of the ignition front expands the fastest in the negative direction of the fuel gradient, which also correlates well with the temperature gradient in unburned gas. In the lower ignition kernel this makes the reaction front to displace along the bowl edge towards the impingement location and here it enters into the experimental plane which is validated in the experiments, cf. figure 5.23. The displacement

speed of the reaction front shows a good qualitative agreement with measured data in the experimental plane.

The experimental data in figure 5.23 shows iso-lines of chemiluminescence signal covering an irregular area rather than a thin reaction zone. In the same figure the consumption of the CH_2O occurs roughly 0.3 crank angles after the chemiluminescence iso-line has reached the region. This implies that the width of the reactivity brush is of the order of several millimetres. Due to the highly turbulent environment and near-stoichiometric mixture an expected flame brush thickness would be at least a magnitude smaller and this was a distributed reaction zone the flame the "islands" of reactivity would be visible in the experiments. This again reinforces the idea that the process is driven by a wide ignition front. A similar consumption delay of CH_2O is observed in the simulations.

The simulated state of combustion at the the peak of ignition is shown in the experimental plane in figure 5.24 where most of the fuel is part of a very wide ignition front. As the premixed combustion fades due to lack of reactants the reactivity brush converges on the stoichiometry with a decreasing brush thickness. At such late stages of the combustion a clear mixing controlled process can be observed, cf. figure 5.25. The mixing controlled combustion in this figure shows a very good qualitative agreement with the experimental chemiluminescence which shows that the mixing model is able to reproduce the location of the stoichiometry even after the density change due to combustion, which validates the model at such late stages.

Both simulations and experiments show that the mixing controlled flame has very low intensity in comparison to the premixed combustion event. This is expected since no spray induced shear layer mixing occurs as in CDC. This highlights a problem with the PPC engine concepts which have issues with combustion efficiency under certain operating conditions. It should be noted that the current study includes a single injection for simplicity of mixing analysis and a split injection strategy would likely alleviate such problems.

The displacement speed of iso-lines of of a specie l can be calculated using the following formulation [83]

$$S_d = \frac{\dot{\omega}_l + D_l}{\rho|\nabla Y_l|} \tag{5.7}$$

where $\dot{\omega}_l$ and D_l is the chemical source term and diffusivity term the species. Since CO iso-surfaces are following the reaction front very close it's possible to estimate the displacement speed of the reaction front this way, see figure 5.21. This figure shows how the distribution of displacement speeds (as calculated from equation 5.7) over an iso surface changes over time. Negative values correspond to formation and positive values to consumption of CO. At the beginning of ignition a fast creation front is seen, which then is rapidly consumed

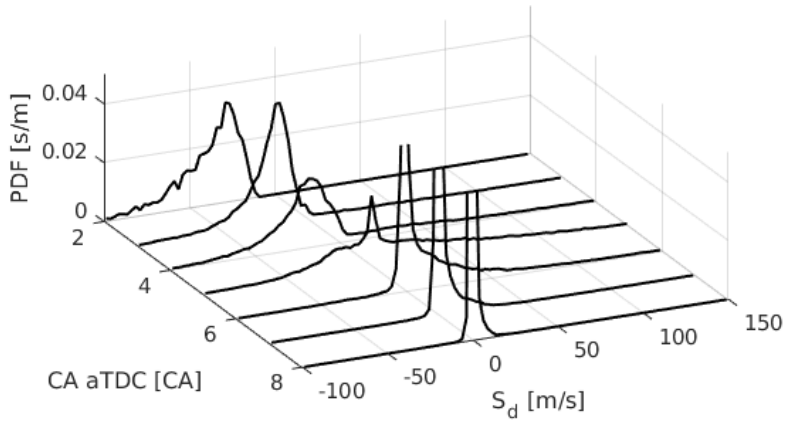

Figure 5.21: Time progression of the distributions of displacement speed of CO during an ignition front. The distribution is taken from iso-lines of CO at 0.05 value.

at 5 CA aTDC. After this the CO iso-lines converge on some location due to the non-premixed flame.

The PaSR approach is successful in modelling the effects of the ignition front and non-premixed combustion. Due to the nature of reaction rate scaling as shown in equation 4.31 the required temperature to obtain ignition in a filtered field has to be artificially increased. Compared to a well stirred reactor simulation the difference was roughly 20 K at the moment of injection. While this temperature offset has some unknown effect on the subsequent combustion the model as a whole is still able to capture essential quantities such as CH_2O formation and destruction, ignition front propagation and mixing controlled reactivity in satisfactory detail.

5.4.2 ESF approach

While transported PDF model approaches are way more expensive than other combustion models they allow for important physical insights such as transported turbulent stratification of scalars. For the modelling of combustion mode transitions from auto-ignition mode to premixed deflagration wave mode such quantities are of utmost importance. The methods described in section 4.5.3 are used to model the combustion process of the Scania D13 engine described in the previous section, with the same grid and the LES formulation.

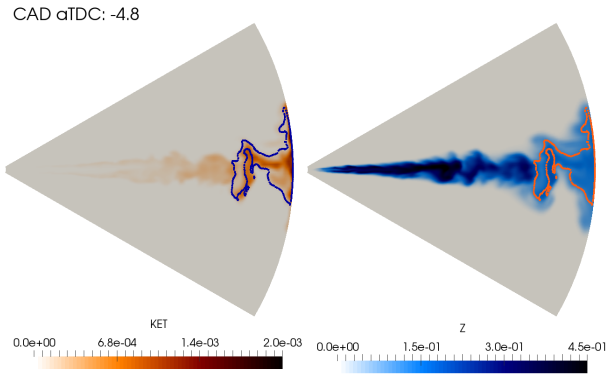

Figure 5.22: $C7KET$ decomposition of the fuel on the left and mixture fraction on the right at -4.8 CA aTDC. The cool flame is shown by a superimposed iso-line of heat release rate. The plane is cut through the center of the spray and its normal is perpendicular to the tangent of the liner.

8 stochastic fields are used to describe the flow.

The results of such a different combustion model are directly noticeable in the required temperature field to obtain combustion, which is considerably lower for the ESF simulation, and also closer to experimental observations. This is due to the large stratification in temperature which allows some of the stochastic instances to ignite earlier than others, cf. figure 5.26. The following premixed reaction front ignites at roughly the same location, but propagates in a thin reaction zone rather than the distributed zone seen in figure 5.24. Reactivity progresses at a faster pace than in the PaSR simulation and shows a higher pressure rise rate, comparable to results seen in WSR approaches. This can possibly be explained by the transported stratification in CO which enables some non-reacting mixtures surrounding the high-temperature zones to react quicker. The standard deviation of the temperature field reaches several hundreds of Kelvin close to the reaction zone as well. A similar transition to non-premixed flame can be observed at 7-8 CA aTDC.

While the ESF results show a good comparison to the optical experiments, just like the PaSR approach, the combustion process shows a faster and more violent ignition, even though the temperature is lower. Due to the violent ignition the combustion phasing does not entirely match the experimental pressure trace. More research is needed to generate a reliable ESF methodology for PPC engine combustion.

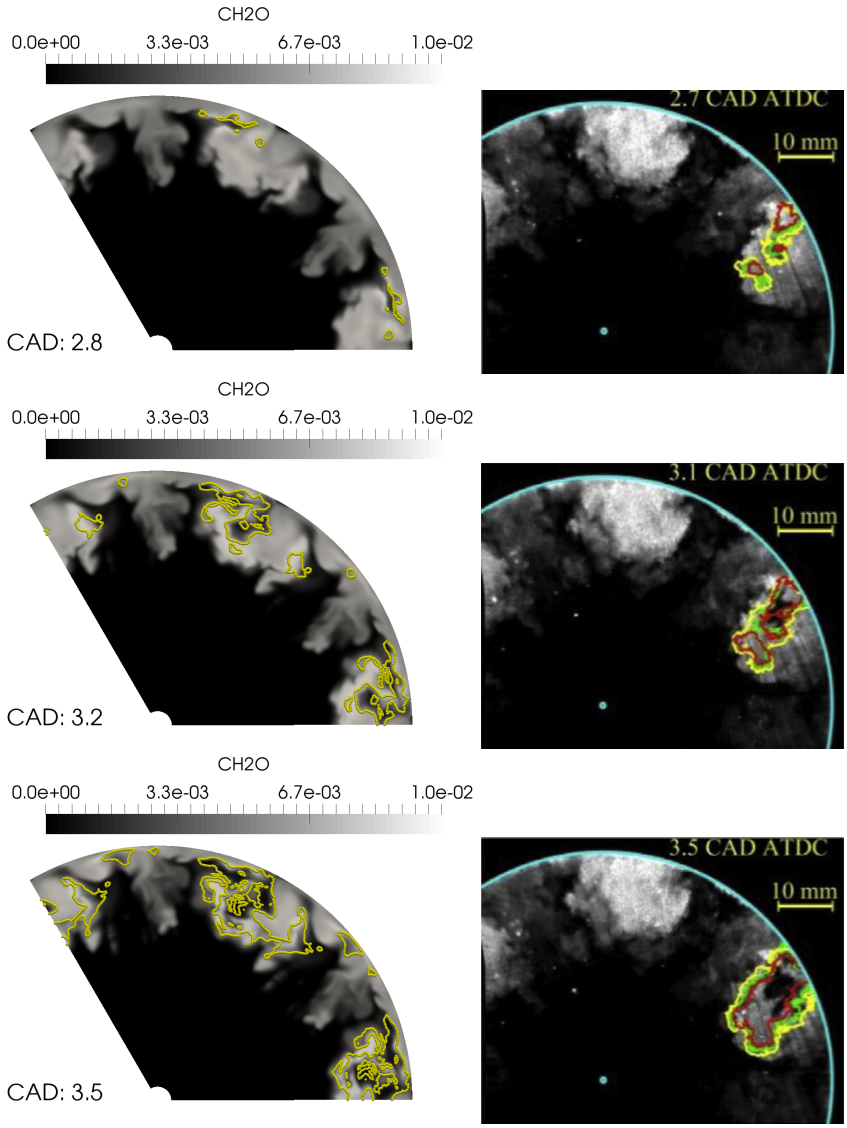

Figure 5.23: A time progression of the reactivity and CH_2O consumption in the experimental plane. Simulated results are found on the left side and experimental values on the right. The yellow lines on the simulated data are isolines of the heat release rate. These lines are intended for comparison with the coloured isolines of chemiluminescence signal overlapping the experimental CH_2O figures. Red, green and yellow lines on the experimental side correspond to -0.3, -0.1 and 0.1 CAD offset to the denoted time. The simulated domain has been periodically replicated to better show the spray-spray interaction.

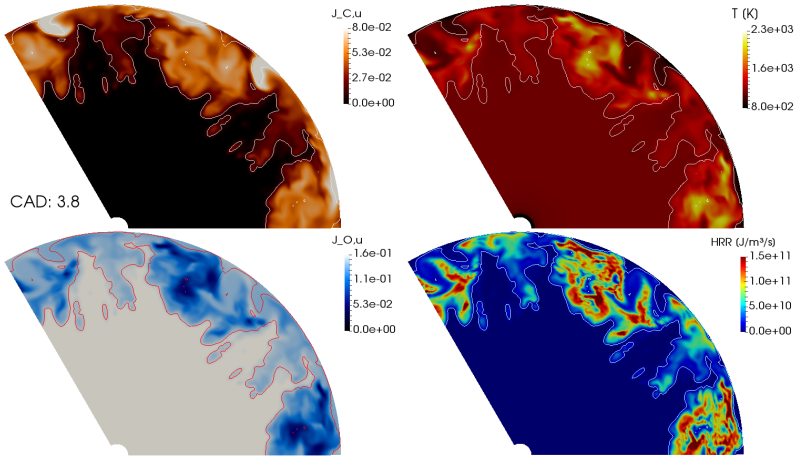

Figure 5.24: The state of combustion in the experimental plane, showing unoxidised carbon, temperature, unoxidised oxygen and heat release rate at the peak heat release rate. Note that nearly all of the fuel clouds shows moderate to high heat release.

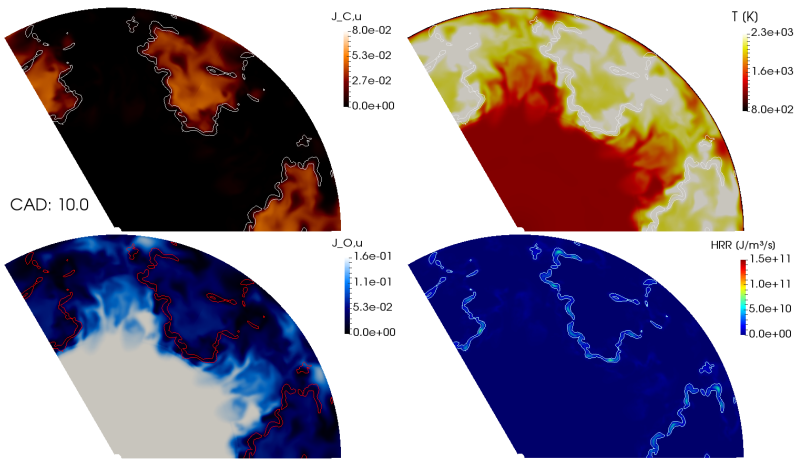

Figure 5.25: Mixing controlled flame at a late stage of combustion. The pictures show unoxidised carbon, temperature, unoxidised oxygen and heat release rate. Nearly all the unoxidised fuel is located on the rich side of stoichiometry. Relatively low levels of mixing (compared to CDC) causes the heat release to be very slow.

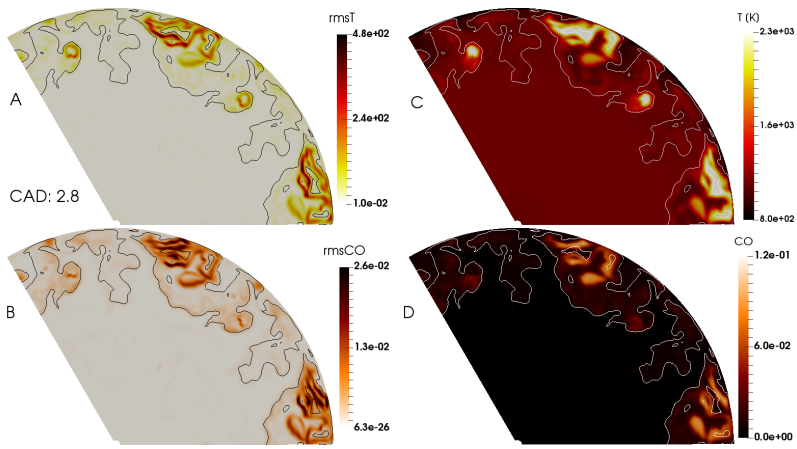

Figure 5.26: The RMS stratification (A) and mean (B) of temperature and RMS stratification (C) and mean (D) of CO at the moment the fuel in the experimental plane ignites in the ESF simulation. Iso-lines of heat release rate are visible.

Chapter 6

Summary

6.1 Concluding remarks and future work

The presented work deals with simulations of partially premixed combustion engines using 3D computational fluid dynamics methods in order to study how the more fundamental aspects of combustion in PPC engines work and how to properly model such physics in filtered flow formulation. The first part of the thesis studies the effects of initial conditions and flow simplifications on the following simulations. Non-reacting cases are studied to observe formation, decay and orientation of large scale flow structures such as swirl in paper I. The effect of flow simplifications and selection of initial conditions on large scale stratification of scalars is studied in paper II. The following conclusions are made when studying the Volvo I5D piston bowl geometry:

- A RAS study presented in paper I shows that the orientation of the rotating large scale structure (combined flow and tumble) is formed early during the gas exchange cycle. The large scale structure is continuously siphoned by turbulence formed due to geometric constraints. The orientation of the large scale structure reaches a maximum tilt in relation to the piston axis close to the intake valve closing event.

- After the intake valve is closed the tumble component of the large scale structure loses magnitude quickly due to the increasingly small cylinder volume. At -30 CAD aTDC the mean field contained no angular momentum in the tumble direction.

- A comparison between laminar initial conditions and highly turbulent initial conditions prior to injection using LES is presented in paper III. The stratification of fuel and temperature close to TDC for three different injection strategies show very little difference.

- By comparing progression of full cylinder LES simulations to periodic sector domains paper III showed that for certain cases where fuel mixing occurs close to the

center of the cylinder large mixing errors are introduced by the periodicity assumption.

The second part of the thesis studied the early combustion process in PPC engines and how it is affected by charge and temperature stratification. Simulations using transported finite rate chemistry yield the following results:

- In paper II a RAS study of the effect of injection timing on ignition and combustion duration shows that ignition modelling accuracy is determined by how well scalar stratification can be modelled in regions lacking large gradients of fuel or temperature.
- The combustion in PPC engines depends on the ignition front mode to a large extent. While early injection strategies cause small stratification in physical properties which affect τ_i the total stratification in τ_i becomes more severe due to the behaviour of chemical kinetics.
- The transition from auto-ignition to flames of some kind is identified as the main source of incomplete combustion in PPC engines using PRF fuel.
- In paper IV an LES-WSR study of the large scale stratification is carried out for locally fuel lean late injections and shows a good agreement with experimental data. This shows that large scale stratification is important for the modelling of ignition fronts in PPC engines and that small scale turbulence is not vital for the auto-ignition part of premixed combustion modelling.
- Paper V uses an LES-PaSR model applied to late injection PPC timing to show that the temporal and spatial progression of reaction fronts can be predicted using a PaSR model for chemistry/turbulence interaction. High temperature reactivity and CH_2O combustion is compared to experimental chemiluminescence and PLIF which validate the results.
- Late stage combustion shows a very slow non-premixed flame which is not entirely combusted at 20 CAD aTDC. This type of late combustion is less thermodynamically efficient and might even be extinguished by the expansion stroke.

The PPC engine concept allows reduced emissions while allowing high compression ratios, but the mixing process should be shortened to obtain more control. This could be achieved through more efficient injectors which mix the fuel in a very short time, allowing more control. The diesel piston bowl causes combustion to occur close to the wall which causes high energy losses.

From a modelling aspect, PPC engines need better treatment of unresolved stratification to properly recreate the ignition front combustion. Transported PDF models or conditional moment closure could be tested to represent auto-ignition better.

Chapter 7

Summary of publications

Paper I: Numerical estimation of asymmetry of in-cylinder flow in a light duty direct injection engine with re-entrant piston bowl

C. Ibron, M. Jangi, T. Lucchini, XS. Bai
SAE Technical Paper, 2017-01-2209

This paper investigates how the swirl flow structure in a light duty engine behaves during compression. A 3D-CFD RAS model treating generic boundary displacement by means of mesh node diffusion is applied in OpenFOAM, resulting in a flow geometry interaction study. The large scale structures of the flow are analysed by means of distribution of angular momentum and by applying a vortex centre identification algorithm on planar velocity fields. The resulting planar flow fields are also compared to experimental PIV measurements and the analysis concludes that asymmetric behaviour of the swirl structure persists into late stages of the compression cycle.

The candidate did the numerical simulations, the analysis and processing of simulated data, the comparison to the optical data. The candidate wrote the paper with assistance from supervisors.

Paper II: Effect of injection timing on the ignition and mode of combustion in a HD PPC engine running low load

C. Ibron, M. Jangi, XS. Bai
SAE Technical Paper, 2019-01-0211

The paper reports on a numerical investigation on the influence of injection timing on combustion in a PPC engine. A 3D-CFD model using RAS turbulence formulation is used to obtain information on spray behaviour, ignition location, the required thermodynamic state for ignition and the heat release rate. The results are compared to data from an

optical engine.

The candidate did the numerical simulations, the data processing, analysis and comparison of data to experimental pictures. Supervisors helped out in data analysis and writing process.

Paper III: Effects of in-cylinder flow simplifications on turbulent mixing at varying injection timings in a piston bowl PPC engine

C. Ibron, M. Jangi, XS. Bai
SAE Technical Paper, 2019-01-0220

This paper discusses how flow assumptions in LES formulation are treated in simulations of PPC engines. A non-reacting simulation of fuel and temperature distribution is run in both full cylinder and sector domains and compared. A second investigation into how initial conditions are affecting PPC engine simulations is performed by comparing an advanced turbulent initial condition with tilted swirl structure to a laminar initial condition with the same swirl number. Results imply the simplifications can be valid for certain conditions.

The candidate did all parts of the work, but received help from supervisors in the writing process.

Paper IV: Large eddy simulation of an ignition front in a heavy duty partially premixed combustion engine

C. Ibron, H. Fatehi, M. Jangi, XS. Bai
SAE Technical Paper, 2019-01-0211

This paper investigates influence of scalar stratification on the speed of ignition fronts in PPC engine simulations. Two injection timings with separate stratification are compared in LES studies in terms of fuel and temperature stratification. The distributions of these scalars are then coupled to the reaction front displacement speed in the engine. Likelihood of ignition front influence is treated in diffusivity/reactivity budget analysis, showing proof of ignition front in the simulation. Results are compared to optical data in terms of pressure rise rate, ignition location and reactivity displacement speed.

The candidate did the numerical simulations, the data processing and analysis, the comparison to optical data and the writing. Supervisors assisted in writing and analysis.

Paper V: Numerical simulation of a mixed-mode reaction front in a PPC engine

C. Ibron, H. Fatehi, Z. Wang, P. Stamatoglou, M. Lundgren, M. Aldén, M. Richter, Ö. Andersson, XS. Bai

Manuscript submitted to the 38th International Symposium on Combustion

This paper reports on a numerical investigation of mixed mode combustion in a heavy duty PPC engine. An LES study of a late PPC injection timing is compared to optical data. The study covers qualitative comparison between simulated and experimental data of ignition location, CH_2O formation and consumption, ignition front displacement speed and non-premixed flame location. Analysis of the partially stirred reactor combustion model's ability to represent turbulence-chemistry interaction is presented. A quantitative estimation of displacement speed is presented.

The candidate did the numerical simulations, data processing, analysis and writing. Supervisors helped out in analysis and writing processes.

References

[1] BP. *Statistical Review of World Energy 2019*. Tech. rep. 2019. URL: https://www.bp.com/content/dam/bp/business-sites/en/global/corporate/pdfs/energy-economics/statistical-review/bp-stats-review-2019-full-report.pdf.

[2] Iain Colin Prentice et al. "The carbon cycle and atmospheric carbon dioxide". In: Cambridge University Press, 2001.

[3] Ottmar Edenhofer et al. *Renewable energy sources and climate change mitigation: Special report of the intergovernmental panel on climate change*. Cambridge University Press, 2011.

[4] IPCC (Intergovernmental Panel on Climate Change). "Special Report, Global Warming of 1.5° C (SR15)". In: (2018).

[5] IPCC. "Mitigation of climate change". In: *Contribution of Working Group III to the Fifth Assessment Report of the Intergovernmental Panel on Climate Change* 1454 (2014).

[6] Mia Romare and Lisbeth Dahllöf. "The life cycle energy consumption and greenhouse gas emissions from lithium-ion batteries". In: *Stockholm. Zugriff am* 23 (2017), p. 2017.

[7] Sara Evangelisti et al. "Life cycle assessment of a polymer electrolyte membrane fuel cell system for passenger vehicles". In: *Journal of cleaner production* 142 (2017), pp. 4339–4355.

[8] Junji Tokieda et al. *„The Mirai–Life Cycle Assessment Report "*. Tech. rep. Technical report, Toyota Motor Corporation. 218 REFERENCES, 2015.

[9] Dominic A Notter et al. "Life cycle assessment of PEM FC applications: electric mobility and μ-CHP". In: *Energy & Environmental Science* 8.7 (2015), pp. 1969–1985.

[10] SR Dhanushkodi et al. "Life cycle analysis of fuel cell technology". In: *Journal of Environmental Informatics* 11.1 (2008), pp. 36–44.

[11] John E Dec. "Advanced compression-ignition engines—understanding the in-cylinder processes". In: *Proceedings of the combustion institute* 32.2 (2009), pp. 2727–2742.

[12] Adam B Dempsey, Scott J Curran, and Robert M Wagner. “A perspective on the range of gasoline compression ignition combustion strategies for high engine efficiency and low NOx and soot emissions: Effects of in-cylinder fuel stratification”. In: *International Journal of Engine Research* 17.8 (2016), pp. 897–917.

[13] Shigeru Onishi et al. “Active thermo-atmosphere combustion (ATAC)—a new combustion process for internal combustion engines”. In: *SAE Transactions* (1979), pp. 1851–1860.

[14] Robert H Thring. *Homogeneous-charge compression-ignition (HCCI) engines*. Tech. rep. SAE Technical paper, 1989.

[15] Kazuhisa Inagaki et al. “Dual-Fuel PCI Combustion Controlled by In-Cylinder Stratification of Ignitability”. In: *SAE 2006-01-0028*. Apr. 2006. DOI: 10.4271/2006-01-0028. URL: http://papers.sae.org/2006-01-0028/.

[16] Gautam T Kalghatgi, Per Risberg, and Hans-Erik Ångström. “Advantages of Fuels with High Resistance to Auto-ignition in Late-injection, Low-temperature, Compression Ignition Combustion”. In: *SAE Technical Paper 2006-01-3385*. SAE International, Mar. 2006. DOI: 10.4271/2006-01-3385. URL: http://dx.doi.org/10.4271/2006-01-3385.

[17] Tsuyoshi Goto et al. “The new Mazda gasoline engine Skyactiv-G”. In: *MTZ worldwide eMagazine* 72.6 (2011), pp. 40–47.

[18] Christian Ibron et al. “Large Eddy Simulation of an Ignition Front in a Heavy Duty Partially Premixed Combustion Engine”. In: *14th International Conference on Engines & Vehicles*. SAE International, Sept. 2019.

[19] Jeffrey D Naber and Dennis L Siebers. “Effects of gas density and vaporization on penetration and dispersion of diesel sprays”. In: *SAE transactions* (1996), pp. 82–111.

[20] Dennis L Siebers. “Scaling liquid-phase fuel penetration in diesel sprays based on mixing-limited vaporization”. In: *SAE transactions* (1999), pp. 703–728.

[21] Jens Eggers and Emmanuel Villermaux. “Physics of liquid jets”. In: *Reports on progress in physics* 71.3 (2008), p. 036601.

[22] Fu-Quan Zhao, Ming-Chia Lai, and David L Harrington. “A review of mixture preparation and combustion control strategies for spark-ignited direct-injection gasoline engines”. In: *SAE transactions* (1997), pp. 861–904.

[23] AD Gosman and D Clerides. “Diesel spray modelling: a review”. In: *Proceedings of ILASS-Europe, Florence, Italy* (1997).

[24] John E Dec and Christoph Espey. “Chemiluminescence imaging of autoignition in a DI diesel engine”. In: *SAE transactions* (1998), pp. 2230–2254.

[25] John E Dec. “A conceptual model of Dl Diesel combustion based on laser-sheet imaging”. In: *SAE transactions* (1997), pp. 1319–1348.

[26] N. Ladommatos et al. “The Dilution, Chemical, and Thermal Effects of Exhaust Gas Recirculation on Diesel Engine Emissions - Part 1: Effect of Reducing Inlet Charge Oxygen”. In: *SAE Technical Paper 961165*. May 1996. DOI: 10.4271/961165. URL: http://papers.sae.org/961165/.

[27] S.L. Plee et al. “Diesel NOx emissions—A simple correlation technique forintake air effects”. In: *Symposium (International) on Combustion* 19 (1982), pp. 1495–1502. DOI: 10.1016/S0082-0784(82)80326-3. URL: https://www.sciencedirect.com/science/article/pii/S0082078482803263.

[28] S. L. Plee, T. Ahmad, and J. P. Myers. “Flame Temperature Correlation for the Effects of Exhaust Gas Recirculation on Diesel Particulate and NOx Emissions”. In: *SAE Transactions* 90 (1981), pp. 3738–3754. DOI: 10.2307/44724998. URL: https://www.jstor.org/stable/44724998.

[29] Magnus Christensen, Bengt Johansson, and Patrik Einewall. “Homogeneous charge compression ignition (HCCI) using isooctane, ethanol and natural gas-a comparison with spark ignition operation”. In: *SAE transactions* (1997), pp. 1104–1114.

[30] Jan-Ola Olsson, Per Tunestål, and Bengt Johansson. “Closed-loop control of an HCCI engine”. In: *SAE Transactions* (2001), pp. 1076–1085.

[31] Magnus Lewander et al. *Evaluation of the operating range of partially premixed combustion in a multi cylinder heavy duty engine with extensive EGR*. Tech. rep. SAE Technical Paper, 2009.

[32] Constantine Arcoumanis and Take Kamimoto. *Flow and combustion in reciprocating engines*. Springer Science & Business Media, 2009.

[33] John E Dec, Wontae Hwang, and Magnus Sjöberg. *An investigation of thermal stratification in HCCI engines using chemiluminescence imaging*. Tech. rep. SAE Technical Paper, 2006.

[34] F. Zhang, R. Yu, and X.S. Bai. “Direct numerical simulation of PRF70/air partially premixed combustion under IC engine conditions”. In: *Proceedings of the Combustion Institute* 35 (Jan. 2015), pp. 2975–2982. DOI: 10.1016/J.PROCI.2014.09.004. URL: https://www.sciencedirect.com/science/article/pii/S1540748914004210.

[35] R. Yu et al. “Effect of Temperature Stratification on the Auto-ignition of Lean Ethanol/Air Mixture in HCCI engine”. In: June 2008. DOI: 10.4271/2008-01-1669. URL: http://papers.sae.org/2008-01-1669/.

[36] Christian Ibron, Mehdi Jangi, and Xue-Song Bai. “Effects of In-Cylinder Flow Simplifications on Turbulent Mixing at Varying Injection Timings in a Piston Bowl PPC Engine”. In: *WCX SAE World Congress Experience*. SAE International, Apr. 2019. DOI: https://doi.org/10.4271/2019-01-0220. URL: https://doi.org/10.4271/2019-01-0220.

[37] W L Hardy and Rolf D Reitz. "A Study of the Effects of High EGR, High Equivalence Ratio, and Mixing Time on Emissions Levels in a Heavy-Duty Diesel Engine for PCCI Combustion". In: *SAE Technical Paper 2006-01-0026*. SAE International, Apr. 2006. DOI: https://doi.org/10.4271/2006-01-0026. URL: https://doi.org/10.4271/2006-01-0026.

[38] Sanghoon Kook et al. "The influence of charge dilution and injection timing on low-temperature diesel combustion and emissions". In: *SAE transactions* (2005), pp. 1575–1595.

[39] WF Colban and PC Miles. *S. oh,"Effect of intake Pressure on Performance and Emissions in an Automotive Diesel Engine Operating in Low Temperature Combustion Regimes"*. Tech. rep. SAE 2007-01-4063, 2007.

[40] Vittorio Manente et al. "An Advanced Internal Combustion Engine Concept for Low Emissions and High Efficiency from Idle to Max Load Using Gasoline Partially Premixed Combustion". In: *SAE Technical Paper 2010-01-2198*. SAE International, Mar. 2010. DOI: 10.4271/. URL: http://dx.doi.org/10.4271/2010-01-2198.

[41] Leif Hildingsson et al. *Fuel octane effects in the partially premixed combustion regime in compression ignition engines*. Tech. rep. SAE Technical Paper, 2009.

[42] Hadeel Solaka. "Impact of fuel properties on partially premixed combustion". PhD thesis. Lund University, 2014.

[43] Mark P.B. Musculus, Paul C. Miles, and Lyle M. Pickett. "Conceptual models for partially premixed low-temperature diesel combustion". In: *Progress in Energy and Combustion Science* 39 (Apr. 2013), pp. 246–283. DOI: 10.1016/j.pecs.2012.09.001. URL: http://linkinghub.elsevier.com/retrieve/pii/S0360128512000548.

[44] Mark C Sellnau et al. *Part-load operation of gasoline direct-injection compression ignition (GDCI) engine*. Tech. rep. SAE Technical Paper, 2013.

[45] Mark C Sellnau et al. "Full-time gasoline direct-injection compression ignition (GDCI) for high efficiency and low NOx and PM". In: *SAE International Journal of Engines* 5.2 (2012), pp. 300–314.

[46] Mateusz Pucilowski et al. "Numerical Investigation of Methanol Ignition Sequence in an Optical PPC Engine with Multiple Injection Strategies". In: *14th International Conference on Engines & Vehicles*. SAE International, Sept. 2019. DOI: https://doi.org/10.4271/2019-24-0007. URL: https://doi.org/10.4271/2019-24-0007.

[47] Shuji Kimura et al. "Ultra-clean combustion technology combining a low-temperature and premixed combustion concept for meeting future emission standards". In: *Sae Transactions* (2001), pp. 239–246.

[48] Shuji Kimura et al. “New combustion concept for ultra clean and high efficiency small DI diesel engine.pdf”. In: *SAE Technical Paper 1999-01-3681*. 1999. ISBN: 0148-7191. DOI: 10.4271/1999-01-3681.

[49] Hiroshimi Yanagihara. “Ignition timing control at Toyota “Unibus” combustion system”. In: *Proc. A new generation of engine combustion processes for the future*. 2001, pp. 35–42.

[50] Dugald Clerk. *Cylinder actions in gas and gasoline engines*. Tech. rep. SAE Technical Paper, 1921.

[51] Slavey Tanov et al. “Effects of Injection Strategies on Fluid Flow and Turbulence in Partially Premixed Combustion (PPC) in a Light Duty Engine”. In: *SAE Technical Paper 2015-24-2455*. SAE International, Mar. 2015. DOI: 10.4271/2015-24-2455. URL: http://dx.doi.org/10.4271/2015-24-2455.

[52] Sara Lonn et al. “Optical Study of Fuel Spray Penetration and Initial Combustion Location under PPC Conditions”. In: *SAE Technical Paper 2017-01-0752*. Mar. 2017. DOI: 10.4271/2017-01-0752. URL: http://papers.sae.org/2017-01-0752/.

[53] Zhenkan Wang et al. “Simultaneous 36□kHz PLIF/chemiluminescence imaging of fuel, CH2O and combustion in a PPC engine”. In: *Proceedings of the Combustion Institute* 37.4 (Jan. 2019), pp. 4751–4758. ISSN: 1540-7489. DOI: 10.1016/J.PROCI.2018.06.019. URL: https://www.sciencedirect.com/science/article/pii/S1540748918302025.

[54] Leilei Xu et al. “Experimental and modeling study of liquid fuel injection and combustion in diesel engines with a common rail injection system”. In: *Applied Energy* 230 (Nov. 2018), pp. 287–304. ISSN: 0306-2619. DOI: 10.1016/J.APENERGY.2018.08.104. URL: https://www.sciencedirect.com/science/article/pii/S0306261918312741.

[55] Hendrik Tennekes et al. *A first course in turbulence*. MIT press, 1972.

[56] Norbert Peters. *Turbulent combustion*. 2001.

[57] R Borghi. “On the structure and morphology of turbulent premixed flames”. In: *Recent advances in the Aerospace Sciences*. Springer, 1985, pp. 117–138.

[58] Ankit Bhagatwala et al. “Numerical investigation of spontaneous flame propagation under RCCI conditions”. In: *Combustion and Flame* 162 (Sept. 2015), pp. 3412–3426. DOI: 10.1016/J.COMBUSTFLAME.2015.06.005. URL: https://www.sciencedirect.com/science/article/pii/S0010218015001844.

[59] Ya.B. Zeldovich. “Regime classification of an exothermic reaction with nonuniform initial conditions”. In: *Combustion and Flame* 39 (Oct. 1980), pp. 211–214. DOI: 10.1016/0010-2180(80)90017-6. URL: https://www.sciencedirect.com/science/article/pii/0010218080900176.

[60] Rixin Yu and Xue-Song Bai. "Direct numerical simulation of lean hydrogen/air auto-ignition in a constant volume enclosure". In: *Combustion and Flame* 160.9 (Sept. 2013), pp. 1706–1716. ISSN: 0010-2180. DOI: 10.1016/J.COMBUSTFLAME.2013.03.025. URL: https://www.sciencedirect.com/science/article/pii/S0010218013001259.

[61] F. Zhang, R. Yu, and X.S. Bai. "Effect of split fuel injection on heat release and pollutant emissions in partially premixed combustion of PRF70/air/EGR mixtures". In: *Applied Energy* 149 (July 2015), pp. 283–296. DOI: 10.1016/J.APENERGY.2015.03.058. URL: https://www.sciencedirect.com/science/article/pii/S0306261915003426.

[62] Evatt R. Hawkes et al. "Direct numerical simulation of ignition front propagation in a constant volume with temperature inhomogeneities: II. Parametric study". In: *Combustion and Flame* 145.1-2 (Apr. 2006), pp. 145–159. ISSN: 0010-2180. DOI: 10.1016/J.COMBUSTFLAME.2005.09.018. URL: https://www.sciencedirect.com/science/article/pii/S0010218005003354.

[63] Jacqueline H Chen et al. "Direct numerical simulation of ignition front propagation in a constant volume with temperature inhomogeneities I. Fundamental analysis and diagnostics". In: *Combustion and Flame* 145 (2006), pp. 128–144. DOI: 10.1016/j.combustflame.2005.09.017. URL: www.elsevier.com/locate/combustflame.

[64] Ramanan Sankaran et al. "The effects of non-uniform temperature distribution on the ignition of a lean homogeneous hydrogen–air mixture". In: *Proceedings of the Combustion Institute* 30.1 (Jan. 2005), pp. 875–882. ISSN: 1540-7489. DOI: 10.1016/J.PROCI.2004.08.176. URL: https://www.sciencedirect.com/science/article/pii/S0082078404002280.

[65] R. Sankaran and H. G. Im. "Characteristics of auto-ignition in a stratified iso-octane mixture with exhaust gases under homogeneous charge compression ignition conditions". In: *Combustion Theory and Modelling* 9.3 (Aug. 2005), pp. 417–432. ISSN: 1364-7830. DOI: 10.1080/13647830500184108. URL: http://www.tandfonline.com/doi/abs/10.1080/13647830500184108.

[66] Hrvoje Jasak and Zeljko Tukovic. "Automatic mesh motion for the unstructured finite volume method". In: *Transactions of FAMENA* 30.2 (2006), pp. 1–20.

[67] Tommaso Lucchini et al. *Automatic mesh motion with topological changes for engine simulation*. Tech. rep. SAE Technical Paper, 2007.

[68] Tommaso Lucchini, Gianluca D'Errico, and Marco Fiocco. *Multi-dimensional modeling of gas exchange and fuel-air mixing processes in a direct-injection, gas fueled engine*. Tech. rep. SAE Technical Paper, 2011.

[69] Joel H Ferziger and Milovan Perić. *Computational methods for fluid dynamics*. Vol. 3. Springer, 2002.

[70] Pierre Sagaut. *Large eddy simulation for incompressible flows : an introduction*. Springer-Verlag, 2006, p. 556. DOI: 10.1007/b137536.

[71] Stéphane Richard et al. "Towards large eddy simulation of combustion in spark ignition engines". In: *Proceedings of the combustion institute* 31.2 (2007), pp. 3059–3066.

[72] Olivier Vermorel et al. "Towards the understanding of cyclic variability in a spark ignited engine using multi-cycle LES". In: *Combustion and flame* 156.8 (2009), pp. 1525–1541.

[73] Rickard Solsjö et al. "Large Eddy Simulation of Partially Premixed Combustion in an Internal Combustion Engine". In: *SAE Technical Paper 2012-01-0139*. Apr. 2012. DOI: 10.4271/2012-01-0139. URL: http://papers.sae.org/2012-01-0139/.

[74] Tobias Joelsson et al. "Large eddy simulation and experiments of the auto-ignition process of lean ethanol/air mixture in HCCI engines". In: *SAE International Journal of Fuels and Lubricants* 1.1 (2009), pp. 1110–1119.

[75] Stephen B Pope. "Ten questions concerning the large-eddy simulation of turbulent flows". In: *New journal of Physics* 6.1 (2004), p. 35.

[76] Peter J O'Rourke. "Statistical properties and numerical implementation of a model for droplet dispersion in a turbulent gas". In: *Journal of Computational Physics* 83 (Aug. 1989), pp. 345–360. DOI: 10.1016/0021-9991(89)90123-X.

[77] Rolf D. Reitz and Jennifer C. Beale. "Modeling spray atomization with the Kelvin-Helmholz/Rayleigh-Taylor Hybrid Model". In: *Atomization and Sprays* 9 (1999), pp. 623–650. DOI: 10.1615/AtomizSpr.v9.i6.40. URL: http://www.dl.begellhouse.com/journals/6a7c7e10642258cc,2b018a87685a3d87,76af95984924bb68.html.

[78] Yao-Dong Liu et al. "Enhancement on a Skeletal Kinetic Model for Primary Reference Fuel Oxidation by Using a Semidecoupling Methodology". In: *Energy & Fuels* 26 (Dec. 2012), pp. 7069–7083. DOI: 10.1021/ef301242b. URL: http://pubs.acs.org/doi/10.1021/ef301242b.

[79] Mehdi Jangi and Xue-Song Bai. "Multidimensional chemistry coordinate mapping approach for combustion modelling with finite-rate chemistry". In: *Combustion Theory and Modelling* 16 (Dec. 2012), pp. 1109–1132. DOI: 10.1080/13647830.2012.713518. URL: http://www.tandfonline.com/doi/abs/10.1080/13647830.2012.713518.

[80] Zhenkan Wang et al. “High-Speed Particle Image Velocimetry Measurement of Partially Premixed Combustion (PPC) in a Light Duty Engine for Different Injection Strategies”. In: *SAE Technical Paper 2015-24-2454*. SAE International, Mar. 2015. DOI: 10.4271/2015-24-2454. URL: http://dx.doi.org/10.4271/2015-24-2454.

[81] Norbert Peters, Bruno Kerschgens, and Günther Paczko. “Super-Knock Prediction Using a Refined Theory of Turbulence”. In: *SAE International Journal of Engines* 6.2 (Apr. 2013), pp. 2013–01. DOI: 10.4271/2013-01-1109. URL: https://www.sae.org/content/2013-01-1109/.

[82] Marcus Olof Lundgren et al. “Effects of Post-Injections Strategies on UHC and CO at Gasoline PPC Conditions in a Heavy-Duty Optical Engine”. In: *WCX™ 17: SAE World Congress Experience*. SAE International, Mar. 2017. DOI: https://doi.org/10.4271/2017-01-0753. URL: https://doi.org/10.4271/2017-01-0753.

[83] Yanzhao An et al. “Homogeneous charge compression ignition (HCCI) and partially premixed combustion (PPC) in compression ignition engine with low octane gasoline”. In: *Energy* 158 (Sept. 2018), pp. 181–191. ISSN: 03605442. DOI: 10.1016/j.energy.2018.06.057. URL: https://linkinghub.elsevier.com/retrieve/pii/S0360544218311228.

Printed by Media-Tryck, Lund 2019 NORDIC SWAN ECOLABEL 3041 0903

Faculty of Engineering
Lund University
ISBN 978-91-7895-322-6
ISSN 0282-1990
ISRN LUTMDN/TMHP-19/1155-SE